Quarterly Technical Report

Growth, Characterization and Device Development in Monocrystalline Diamond Films

Supported under Grant #N00014-93-I-0437
Office of the Chief of Naval Research
Report for the period 1/1/95–3/31/95

R. F. Davis, J. T. Glass, and R. J. Nemanich*
K. S. Ailey, F. R. Sivazlian and S. D. Wolter
North Carolina State University
c/o Materials Science and Engineering Department
*Department of Physics
Raleigh, NC 27695

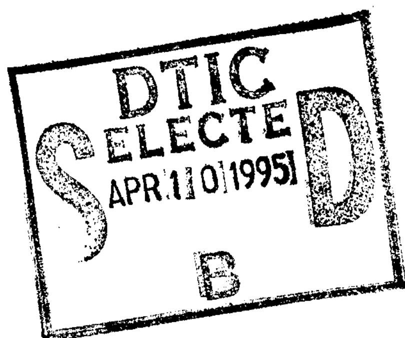

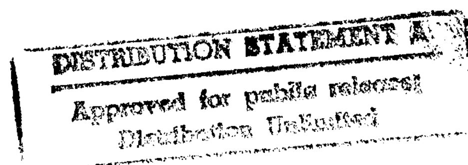

DTIC QUALITY INSPECTED 5

March, 1995

19950407 102

REPORT DOCUMENTATION PAGE

Form Approved
OMB No. 0704-0188

Public reporting burden for this collection of information is estimated to average 1 hour per response, including the time for reviewing instructions, searching existing data sources, gathering and maintaining the data needed, and completing and reviewing the collection of information. Send comments regarding this burden estimate or any other aspect of this collection of information, including suggestions for reducing this burden to Washington Headquarters Services, Directorate for Information Operations and Reports, 1215 Jefferson Davis Highway, Suite 1204, Arlington, VA 22202-4302, and to the Office of Management and Budget Paperwork Reduction Project (0704-0188), Washington, DC 20503.

1. AGENCY USE ONLY *(Leave blank)*

2. REPORT DATE
March, 1995

3. REPORT TYPE AND DATES COVERED
Quarterly Technical 1/1/95–3/31/95

4. TITLE AND SUBTITLE
Growth, Characterization and Device Development in Monocrystalline Diamond Films

5. FUNDING NUMBERS
s400003srr14
1114SS
N00179
N66005
4B855

6. AUTHOR(S)
Robert F. Davis, J. T. Glass and R. J. Nemanich

7. PERFORMING ORGANIZATION NAME(S) AND ADDRESS(ES)
North Carolina State University
Hillsborough Street
Raleigh, NC 27695

8. PERFORMING ORGANIZATION REPORT NUMBER
N00014-93-I-0437

9. SPONSORING/MONITORING AGENCY NAMES(S) AND ADDRESS(ES)
Sponsoring: ONR, Code 314, 800 N. Quincy, Arlington, VA 22217-5660
Monitoring: Admin. Contracting Officer, ONR, Regional Office Atlanta
101 Marietta Tower, Suite 2805
101 Marietta Street
Atlanta, GA 30332-0490

10. SPONSORING/MONITORING AGENCY REPORT NUMBER

11. SUPPLEMENTARY NOTES

12a. DISTRIBUTION/AVAILABILITY STATEMENT
Approved for Public Release; Distribution Unlimited

12b. DISTRIBUTION CODE

13. ABSTRACT *(Maximum 200 words)*

Research continued in the growth of boron nitride films on various substrates including Si(100), diamond (100), Cu(100) and Ni(100) via ion beam assisted electron beam evaporation. Fourier transform infrared spectroscopy and high resolution transmission electron microscopy showed that the total films on Si and diamond consisted of the sequence from the substrate: a-BN, h-BN, c-BN. The c-BN layers formed as a function of deposition temperature, ion current and thickness. The occurrence of this layer is attributed to increasing intrinsic biaxial compressive stress generated during deposition. The interface and surface structure of highly oriented diamond films were examined by low resolution transmission electron microscopy (LRTEM), high resolution transmission electron microscopy (HRTEM) and using a transmission electron microscope with *in situ* cathodoluminescence. Interface studies by HRTEM indicated that SiC formation may have assisted in the formation of highly oriented diamond. Additionally, in some areas diamond appeared to be in direct contact with the silicon substrate; no indication of an amorphous or crystalline interlayer was observed. The grain boundaries of the highly oriented {100} diamond particles observed by LRTEM showed that the misorientation between these particles was compenseated by a series of parallel dislocations. Finally, TEM/CL results showed that the majority of luminescence in the plan view was from misoriented or highly defective diamond grains.

14. SUBJECT TERMS
diamond, cubic boron nitride, ion beam assisted deposition, Fourier transform infrared spectroscopy, plan view TEM studies, highly oriented diamond, cathodoluminescence

15. NUMBER OF PAGES
53

16. PRICE CODE

17. SECURITY CLASSIFICATION OF REPORT	18. SECURITY CLASSIFICATION OF THIS PAGE	19. SECURITY CLASSIFICATION OF ABSTRACT	20. LIMITATION OF ABSTRACT
UNCLAS	UNCLAS	UNCLAS	SAR

Table of Contents

I.	Introduction	1
II.	TEM Studies of Highly Oriented Diamond on Silicon	3
III.	Growth and Characterization of Cubic Boron Nitride Thin Films	37
IV.	Distribution List	53

Accession For
NTIS GRA&I ☑
DTIC TAB ☐
Unannounced ☐
Justification
By
Distribution/
Availability Codes
Dist | Avail and/or Special
A-1

I. Introduction

Diamond as a semiconductor in high-frequency, high-power transistors has unique advantages and disadvantages. Two advantages of diamond over other semiconductors used for these devices are its high thermal conductivity and high electric-field breakdown. The high thermal conductivity allows for higher power dissipation over similar devices made in Si or GaAs, and the higher electric field breakdown makes possible the production of substantially higher power, higher frequency devices than can be made with other commonly used semiconductors.

In general, the use of bulk crystals severely limits the potential semiconductor applications of diamond. Among several problems typical for this approach are the difficulty of doping the bulk crystals, device integration problems, high cost and low area of such substrates. In principal, these problems can be alleviated via the availability of chemically vapor deposited (CVD) diamond films. Recent studies have shown that CVD diamond films have thermally activated conductivity with activation energies similar to crystalline diamonds with comparable doping levels. Acceptor doping via the gas phase is also possible during activated CVD growth by the addition of diborane to the primary gas stream.

The recently developed activated CVD methods have made feasible the growth of polycrystalline diamond thin films on many non-diamond substrates and the growth of single crystal thin films on diamond substrates. More specifically, single crystal epitaxial films have been grown on the {100} faces of natural and high pressure/high temperature synthetic crystals. Crystallographic perfection of these homoepitaxial films is comparable to that of natural diamond crystals. However, routes to the achievement of rapid nucleation on foreign substrates and heteroepitaxy on one or more of these substrates has proven more difficult to achieve. This area of study has been a principal focus of the research of this contract.

At present, the feasibility of diamond electronics has been demonstrated with several simple experimental devices, while the development of a true diamond-based semiconductor materials technology has several barriers which a host of investigators are struggling to surmount. It is in this latter regime of investigation that the research described in this report has and continues to address.

In this reporting period, interface and surface structure of highly oriented diamond films were examined by low resolution transmission electron microscopy, high resolution transmission electron microscopy and using a transmission electron microscopy with *in situ* cathodoluminescence. Continued research was also conducted in the growth of boron nitride films on various substrates including Si(100), diamond (100), Cu (100) and

Ni(100) via ion beam-assisted electron beam evaporation. Fourier transform infrared spectroscopy and high resolution transmission electron microscopy were employed for the characterization of the a-BN, h-BN and c-BN films which were deposited.

The following subsections detail the experimental procedures for each of the aforementioned studies, discuss the results and provide conclusions and references for these studies. Note that each major section is self-contained with its own figures, tables and references.

II. TEM Studies of Highly Oriented Diamond on Silicon

F. R. Sivazlian and S. D. Wolter

North Carolina State University, Dept. of Materials Engineering, Raleigh, NC 27695-7919

B. R. Stoner and J. T. Glass

Kobe Steel USA Inc., PO Box 13608, Research Triangle Park, NC 27709

R. J. Graham

Center for Solid State Science, Arizona State University; Tempe, Arizona 85287-1704*

Abstract

The interface and surface structure of highly oriented diamond films were examined by low resolution transmission electron microscopy (LRTEM), high resolution transmission electron microscopy (HRTEM) and using a transmission electron microscope with *in situ* cathodoluminescence. Interface studies by HRTEM indicated that SiC formation may have assisted in the formation of highly oriented diamond. Additionally, in some areas diamond appeared to be in direct contact with the silicon substrate; no indication of an amorphous or crystalline interlayer was observed. The grain boundaries of the highly oriented {100} diamond particles observed by LRTEM showed that the misorientation between these particles was compensated by a series of parallel dislocations. Finally, TEM/CL results showed that the majority of luminescence in the plan view was from misoriented or highly defective diamond grains.

* current address: NanoTEM Inc.; 7620 McKellips Rd, Suite #419; Scottsdale, AZ 85257

To be submitted to Diamond and Related Materials

Introduction

Diamond has been widely recognized as a suitable material for high temperature, high power, and/or high frequency semiconducting devices due to its exceptional properties such as a wide band gap and low resistivity [1]. Before active elctronic diamond devices can be realized however, single crystal or high quality polycrystalline diamond must be obtained at a low cost. Currently, chemical vapor deposition (CVD) has been utilized to produce, {100} highly oriented diamond by several research groups [2-5] These diamond films have shown considerable improvement in electronic properties over randomly oriented polycrystalline diamond[6]. However, they have not yet attained the quality of high pressure high temperature single crystal or natural diamond and it appears that the low angle grain boundary formation is still limiting the transport properties of these highly oriented films.

Numerous studies on diamond thin film formation have utilized TEM to study interface and defect structures in hopes of improving the understanding of the diamond growth process and the effects of various defects on film properties. Specifically, previous TEM work has given insight into the diamond/substrate interface, the structure of the grains and the grain boundaries as well as the various types of defects which form during nucleation and growth. Cross-sectional TEM observation in particular has been utilized to observe the film/substrate interface and to compliment extensive studies of diamond nucleation processes. Williams et al.[7] studied the effect of growth conditions on the formation of an interfacial layer between the diamond film and the substrate. Using HRTEM, these authors observed that by scratching the substrate (as a nucleation pretreatment method) and using low methane concentrations, a SiC layer formed between the substrate and the diamond. TEM diffraction patterns indicated that under

certain growth conditions the SiC was oriented with respect to the silicon. The formation of this SiC layer was attributed to the low methane concentration, 0.3%, which in turn induced a lower growth rate and allowed more time for a stable interlayer to form. Using higher methane concentrations, 2.0%, the SiC interfacial layer was not observed[8, 9], but rather a thinner layer attributed to either ion beam damage[8] or amorphous silicon formed during the initial stages of growth[10]. J. S. Ma et al. [10] noted that this interfacial layer was located off center between the diamond grains and the substrate but was absent at the nucleation point of the diamond. G. W. Ma et al.[11], however, proposed that the diamond/silicon mismatch might be accounted for by an interlayer of damaged silicon which formed during the initial stages of growth.

These results left several unanswered questions regarding the conditions under which diamond may nucleate epitaxially with respect to the substrate: 1) Is either an amorphous or crystalline interlayer necessary for diamond nucleation? 2) What attribute of the substrate aides in the nucleation and growth of diamond (i.e. carbide forming nature)? 3) Could diamond be grown epitaxial on a silicon substrate? 4) Does SiC play a role in diamond nucleation on silicon? In an attempt to answer some of these questions, an experiment was performed involving diamond growth on single crystal SiC using bias enhanced nucleation. Initial results indicated that approximately 50% of the diamond grains were oriented with respect to the underlying SiC[4]. Cross-sectional HRTEM confirmed that the grains were epitaxial and that the 15% misfit between the diamond and the silicon carbide was not relieved by an amorphous transition layer but rather by a series of misfit dislocations, one approximately every six atomic distances[12]. The next report of textured diamond growth was by Wolter et al.[2] using a multi-step

nucleation and growth process which involved an in-situ carburization followed by the same bias-enhanced nucleation process utilized by Stoner et al.[4] The interfaces of these films will be reported here.

Plan view TEM studies on CVD diamond has included studies of film defects[13, 14] and relative defect densities as a function of growth conditions[11, 15-20]. On {100} textured diamond films with no specific orientation to the substrate, Clausing and coworkers demonstrated that the density of intragranular defects such as twins and stacking faults were much lower for growth on {100} as compared to the {111} planes[17]. The investigation further determined that while the {100} oriented grains were relatively defect free, grain boundaries often contained dense networks of extended defects including dislocations and microtwins. Similar results were confirmed by several other research groups[18-20]. While investigations to determine the types of intragranular defects were being pursued, specific information on the structure of the grain boundaries was unreported. Fallon and Brown investigated these boundaries using HRTEM[21] and parallel electron energy loss spectroscopy (PEELS). They reported that in areas where there was no diamond grain overlap, amorphous carbon was detected at the boundary. In this research, plan view TEM was used to examine the grain structure and boundaries in highly oriented, {100} textured diamond films. The density and location of defects in these films will be discussed. Additionally, low angle {100} grain boundaries will be examined to determine the amount of misorientation resulting from these defects.

Experimental

Samples were grown in an ASTeX® microwave plasma chemical vapor deposition system on [001] silicon substrates. Deposition involved a multi-step process, first reported by Wolter et al[2] which incorporated bias-enhanced nucleation to form the diamond nuclei. Typical nucleation parameters involved a methane and hydrogen gas mixture and a pressure of 15 torr. Bias voltages were approximately -250 volts and methane concentrations varied between 2% and 5%. The substrate temperature was maintained between 750°C and 900°C.

Both cross-sectional and plan view samples were prepared using a standard technique of polishing, dimpling and finally ion milling. This technique for diamond thin films has been explained extensively in a previous work[16] and only the main points will be mentioned here. For cross-sectional samples, a diamond thickness of less than 2μm is preferred for effectively preparing and imaging the interfaces. Thicker samples can be prepared but due to the extreme difference in hardness between the diamond and the substrate, ion milling often removed the substrate before adequately thinning the diamond overlayer; hence, the absence of an interface for observation.

TEM sample preparation involved a multi-step process. Initially, samples were cut into 2 mm x 4 mm pieces and glued together using a viscous 2-part epoxy, Gatan G-1. A thick epoxy was important since the diamond surface is often rough and a thin epoxy will tend to remain only in the crevasses not providing sufficient adhesion on the surface. Samples were mechanically polished to <100μm before being transferred to a VCR wheel dimpler. Dimpling reduced ion milling time and, hence, damage to the sample. Approximately 90μm were dimpled, or until the silicon substrates

became transparent to light, appearing as a red/orange color. At this point samples were mounted on copper rings and ion milled at an angle of 12-15° at 6V until penetration and forming a "diamond bridge". The samples were found to be sufficiently thin when this "bridge" is broken. Further milling at an angle of approximately 9° at 3V for 45 minutes was utilized in order to obtain a large thin area. Plan view samples were prepared by a similar method except that polishing and dimpling were only performed on the silicon side of the sample. Ion milling occurred from either the substrate surface or from both sides depending on what type of information was to be obtained. Milling on both sides of the sample was incorporated to save time during preparation.

Four different transmission electron microscopes were used in this research depending on the microscope resolution or the analytical capabilities necessary. The first, a 200 kV Hitachi H-800 microscope had a maximum magnification of 300, 000 times. In addition, this microscope had a large tilting capability, ±60°, and the capability of scanning transmission electron microscopy (STEM) and energy dispersive x-ray spectroscopy (EDS). This microscope was used if lattice imaging or microdiffraction was not necessary. A 120 kV Philips EM400T analytical microscope, located at Arizona State University equipped with an *in situ* cathodoluminescence (CL) was also capable of spectral resolution and detection in the 300-900nm range, was also used. A detailed description of the system has been referenced previously[22]. Two TOPCON 002B high resolution TEMs (HRTEM) were also used, this will be discussed in more detail later. One was specifically designed for high resolution work with a point to point resolution of 1.8 Å and a lattice resolution of 1.4 Å, the TEM probe feature can image an area between 2.0 nm and 56.0 nm. The maximum magnification was 1,600,000x with a specimen

stage tilt of ± 10°. The second TOPCON 002B was essentially identical to the first 002B but incorporates a thin window EDS system that may detect elements as light as boron. Several specifications were slightly different, the point to point resolution was 2.4 Å while the lattice resolution was identical, 1.4Å. Here, the TEM probe images between 1.2 nm and 33.0 nm with the maximum magnification at 1,300,000x. Another significant difference was the tilt which could be increased three times to ±30°. The microscopes were used interchangeably, depending on availability, except in cases where a larger tilt was necessary or a smaller point to point resolution was necessary.

The CL system used in this study was attached to a Philips 400T transmission electron microscope. This system was capable of obtaining CL spectra and monochromatic CL images of small regions on a sample and imaging the sample region by TEM. The monochromatic CL images were obtained using a STEM attachment and a multi-channel analyzer. Table I shows various types of defects associated with particular CL wavelengths that are relevant to this work[22-26]. This technique is extremely helpful for determining where electrically active defects are located in the material and imaging these defects via TEM.

Results and Discussion

I. Cross-sectional TEM results

The interface between the silicon and the highly oriented diamond (HOD) was investigated by cross-sectional TEM. HRTEM results as well as transmission electron diffraction (TED) patterns were examined to understand the structure of the interface as well the initial stages of highly

oriented diamond nucleation and growth. Previous results had indicated that a SiC interlayer appears to form prior to diamond nucleation[2]. Previous results also indicated an epitaxial relationship between diamond and SiC [12]. Interfaces were therefore examined for the presence of a SiC interlayer . Two additional attributes were investigated; the substrate roughness since the growth process incorporated bias-enhanced nucleation which has been shown to cause substrate etching[27] and, secondly, defects at the crystalline interface due to the large lattice mismatch between Si/SiC and Si/diamond.

Results from TEM selected area diffraction patterns at the sample interface indicated that epitaxial crystalline SiC did form (Figure 1a). From the diffraction pattern, it should be noted that the inner spots represent silicon, the second innermost set of spots represents the silicon carbide and the third ring of spots represents the diamond. A schematic showing the diffraction spots with the corresponding materials and their characteristic plane is shown in figure 1b. The alignment of the silicon and the silicon carbide spots indicates an epitaxial relationship between the two materials. The set of diamond spots is not as definitive. It appears that there are several grains represented in this diffraction pattern but most notably one of the grains is tilted approximately six degrees with respect to the silicon carbide. Similar results have been reported for diamond growth on single crystal silicon carbide[12].

High resolution TEM was also used to analyze the interlayer between the silicon substrate and diamond film. Figure 2 shows a HRTEM image of the sample interface. The micrograph shows that islands of crystalline SiC form as opposed to a uniform crystalline layer. The islands vary in thickness from 0-50 Å. The interface between the silicon and the silicon carbide is therefore not continuous and appears to be highly defective. Similar results

have been previously reported for SiC growth on single crystal silicon[28]. Figure 3 is a HRTEM image of the non-uniform diamond/silicon interface. In this micrograph, the interlayer structure appears to contain crystalline SiC as well as highly defective regions of both silicon and silicon carbide, as indicated on the figure. This defective region is surrounded by crystalline areas and there appears to be some order to the lattice planes. Since this SiC region is considerably thinner than the one shown in the figure 2, the highly defective nature of the layer is not surprising. The defects might have resulted from ion milling damage during sample preparation[28], insufficient time for carbide formation, ion bombardement during the bias-enhanced nucleation proces, and/or stress resulting from the large lattice mismatch. The most probable explanation is insufficient time for carbide formation since both ion milling and bias damage or the large lattice mismatch would be expected to produce a uniformly defective layer.

Several of the areas in these micrographs also indicated that the diamond was in direct contact with the silicon. In figure 4a, lattice fringes from the diamond and silicon are in direct contact with one another and continuous across the interface. Here, the angle between the diamond {111} planes and the silicon {111} planes is approximately 14°, other results from separate samples indicated approximately the same misorientation between diamond and silicon. Considering the mismatch between the diamond, a = 3.51Å, and silicon, a = 5.45Å, is approximately 35%, this is not surprising. A schematic showing the effect of several different angular tilts of diamond with respect to the silicon is shown in figure 4b. Figure 4b (i) shows the effect of completely epitaxial diamond. In this figure, there are approximately five silicon planes for every seven diamond planes. With a 15 degree offset, shown in (ii) and similar to what was observed in the HRTEM, there is not a

significant reduction in the amount of mismatch. However, if there is a 45 degree offset, shown in (iii), the planes appear to line up almost epitaxially with the diamond. A 45 degree tilt of the diamond (100) planes would mean a (110) diamond growth surface. Comparing the relative lattice spacing of (110) diamond, 3.85 Å, to silicon (100), 3.51Å, means a reduction in mismatch from 34% to 7%. This would appear to considerably reduce the strain in the films and would appear to be easier to form epitaxially compared with (100) diamond. However, recent modeling experiments by Tucker et al.[29] confirm that a direct epitaxial alignment is more stable compared to a 45° tilt, acheiving a 3:2 (silicon planes to diamond planes) structure. The authors also indicated that a 9.5° tilt of the diamond would be ideal in acheiving the 3:2 structure, reducing the misfit further.

There are several possible explanations for the existence of diamond directly epitaxial with the silicon. Careful examination of the silicon substrates shows that the silicon surface is rough, unlike the pristine silicon prior to diamond growth. This suggests that during deposition, etching of silicon and/or SiC is occurring, most likely during biased-enhanced nucleation[27]. Etching of the silicon which then recrystallizes to form defective silicon may explain the defective silicon shown on the upper layer of the substrate and the nonuniform SiC layer shown in figure 2. The nonuniform SiC could be attributed to silicon carbide etching during biased-enhanced nucleation resulting in free carbon to be used in the formation of a stable diamond clusters thereby leaving behind only small regions of SiC. Finally, however, diamond may simply be nucleating directly on the silicon substrate. This is suggested by excessive amounts of dislocations at the interface (expected from the large mismatch) and the pristine appearance of the silicon and diamond which do not indicate etching and/or

recrystallization of the growth surface. More data is necessary to determine which of these is more likely to occur.

Low angle grain boundaries were also observed via cross-sectional TEM. In figure 5a two highly oriented diamond grains are misoriented 10° with respect to each other. These grains were examined in the regions where the defects were formed as well as which plane they formed along. The white arrows on the figure indicate where the dislocations formed. In figure 5b a schematic was drawn in order to visualize the grain boundary better. In this schematic the mismatch appears to fall along the {111} plane. However, it is difficult to determine if this schematic is accurate since the exact growth nature of these grains is not fully known and computer modeling of the boundary was not attempted.

II. Plan View TEM of Highly Oriented Diamond

A study of the grain boundaries of HOD was used to gain information on the structure of the boundary and defects that are formed on these boundaries. An SEM image showing the surface of the diamond film used for this study is shown in figure 6. From this micrograph it is obvious that the grains are highly oriented and many appear to have coalesced, as indicated by the arrows. In previous[17] work on randomly oriented polycrystalline {100} faceted diamond films, various defects including microtwins were observed at the boundary regions. A TEM micrograph from the highly oriented film used in this study is shown in figure 7. In this figure one observes several lines of dislocations, indicative of grain boundaries similar to the ones shown in figure 6. Electron diffraction patterns indicated that most boundaries were along the <110> direction as shown in the large area in figure 8. In figure 7 however, boundaries in both the <110> and <100>

direction are observed, as indicated by the respective arrows on the micrograph. A low angle grain boundary was observed at high magnification, figure 9. As is common for low angle grain boundaries[30], a series of distinctive dislocations are seen, indicated by the arrows (one arrow approximately every 5 dislocations). The spacing between each of the dislocations is about 20 nm.

The rotation between grains was measured two ways, calculations using the Burgers vector in conjunction with the dislocation spacing and secondly from the diffraction pattern. In figure 9, it is observed that the dislocations are widely spaced, indicative of a small degree of rotation. The Burgers vector was determined to be a $\frac{1}{2}$ [110] type dislocation from the g•b analysis. The angle of rotation between grains was calculated using the expression[31]; $\varnothing \approx \frac{b}{d}$, where Ø is the degree of rotation, b is the Burgers vector and d is the dislocation spacing. From this equation the rotation between grains was calculated as ≈ 1°. Similar results have been reported in GaAs, also with a diamond cubic type structure[32]. Additionally, from close examination of the electron diffraction pattern the tilt between the two grains (see inset in figure 9) was also measured. By moving from one grain to another the {220} diffraction spot was observed to shift slightly, indicative of a misorientation between the two grains. Using the diffraction pattern at the grain boundary, the angle between the two {220} spots was measured to give the tilt between the two grains. This result corresponds to the tilt measured by Burgers vector calculations. Several grains were measured and the angle was consistently between 0 and 6 degrees. These measurements corroborate previous measurements of the misorientation of diamond films on silicon via x-ray pole figure analysis[33] and previous results using cross-sectional

TEM of epitaxial diamond on single crystal ß-SiC[4]. It is also consistent with observations of the edges of the grains via SEM as was shown in figure 6.

In order to better visualize this and other grain boundaries, a ball and stick model was created of a grain boundary (figure 10). Here two grains are misoriented with respect to each other by 15 degrees; the large distortion was necessary to show more than one dislocation. The black arrows indicate the rows of extra atoms that are added to accommodate for the rotation. In this picture it is seen that even a small amount of distortion between grains can cause extreme distortion on an atomic scale.

Therefore by growing under conditions which promote (100) texture, defects will reside primarily at or near the grain boundaries since (100) diamond surfaces yield low defect densities. With the density of twins and stacking faults reduced within the grains of randomly oriented diamond, point defects and dislocations become the factors limiting the electronic transport properties of the (100) textured, polycrystalline diamond films. The defect densities at the grain boundaries are further reduced by depositing a film that is both (100) textured and highly oriented. This decreases the defect density at the grain boundaries to a series of parallel dislocations at many of the boundaries. Boundaries of this type are more coherent and thus result in improved elctronic transport properties.

III. Cathodoluminescence

Further investigation of these defects utilized *in situ* CL. This technique was used to determine the relative amount of electrically active defects in different regions of the sample and also to specifically image where these defects were located using TEM. First a CL spectra was taken over a relatively large region of the sample to determine the overall characteristics

of the film (figure 11a). An enlargement of the spectral region of interest is shown in figure 11b. A broad band peak appears at approximately 433 nm. This wavelength was utilized for the imaging (figure 12a) because it has been found to be associated with dislocations[34, 35]. The large bright area at the bottom of the image is attributed mainly to increased sample thickness as opposed to an excess of defects. An enlargement of an area of interest is shown in figure 12b. The TEM image from this area is shown in figure 13. A comparison of these TEM and CL images indicates that the majority of the luminescence originates from grains that are not {100} oriented. An apparent low angle grain boundary was then investigated. After extensive tilting and from diffraction patterns, the TEM image in figure 14 showed no defects on the boundaries between the grains, indicative of no azimuthal misorientation between grains. The CL spectra from this region corraborated these results, no luminescence from the grain boundaries was observed in the 300-900nm range, figure 15. However, a significant increase in luminescence was observed in the lower edge of the micrograph where a highly twinned area is located.

Conclusions

{100} highly oriented diamond films grown on (001) silicon via bias-enhanced MPCVD were examined by transmission electron microscopy in the cross-sectional and plan views. Insight was obtained into the interfaces between the diamond and the silicon substrate as well as the interfaces between highly oriented diamond grains.

Cross-sectional HRTEM along with TED patterns verified that SiC was formed at some point during the deposition process. The layer was

nonuniform over the growth surface ranging in thickness from 0-50 nm. These results and the uneven silicon substrate surface seem to indicate that etching is occurring at some point during the growth process, most likely during the initial biasing step. In some areas, the diamond {111} planes were in direct contact with the {111} planes of the silicon substrate. In these cases the diamond grain was tilted between 9-14 degrees with respect to the silicon. This slightly reduced the large lattice mismatch that would occur if the diamond was oriented perfectly with the underlying substrate and, additionally, is consistent with recent work predicting an energetically stable 3:2 arrangement of lattice planes.

At low magnification, plan view observation indicated that {100} grains had grown together to form irregular grain boundaries. These boundaries lie primarily along the <110> but highly defective <100> boundaries are also observed. At higher magnifications parallel dislocations with $\frac{1}{2}[110]$ Burgers vectors were observed at grain boundaries, indicative of a low angle grain boundary. To confirm the misorientation, calculations utilizing both the Burgers vector and electron diffraction patterns determined a tilt of $\approx 1^\circ$ for the example shown here. Several different low angle grain boundaries were observed and the tilt was determined to be between 0 and 6 degrees, varying from grain to grain. *In situ* TEM CL indicated that the majority of electrically active defects were located in highly twinned regions and regions without {100} orientation; defect free boundaries were without luminescence in the 300-900 nm wavelength range.

For highly oriented films to become viable alternatives to single crystals as substrate material for active electronic devices, misorientation and the corresponding defects need to be further reduced. Future experiments should study the effect of misorientation and defect density on the resulting

electronic properties in an attempt to further improve the quality of heteroepitaxial diamond films.

Acknowledgments

This research was supported by BMDO-IST through ONR. All of the CL work was performed at the Center for High Resolution Electron Microscopy, which is supported by the National Science Foundation under grant No.DMR-9115680.

Bibliography

1. A. T. Collins, Semicond. Sci. Technol., **4**, 605-611 (1989).

2. S. D. Wolter, B. R. Stoner, J. T. Glass, P. J. Ellis, D. S. Buhaenko, C. E. Jenkins & P. Southworth, Appl. Phys. Lett., **62**, 1215-1218 (1993).

3. X. Jiang & C.-P. Klages, Diamond and Related Materials, **2**, 1112-1113 (1993).

4. B. R. Stoner & J. T. Glass, Appl. Phys. Lett., **60**, 698-700 (1992).

5. R. Kohl, C. Wild, N. Herres, P. Koidl, B. R. Stoner & J. T. Glass, Appl. Phys.. Lett., **63**, 1792-1794 (1993).

6. B. A. Fox, B. R. Stoner, D. M. Malta, P. J. Ellis, R. C. Glass & F. R. Sivazlian, Diamond and Related Materials, **3**, 382-387 (1994).

7. B. E. Williams, D. A. Asbury & J. T. Glass in **The Physics and Chemistry of Carbides; Nitrides and Borides** , edited by R. Freer (Kluwer Academic Publishers, Published in the Netherlands, 1990) p. 169-181.

8. B. E. Williams, J. T. Glass, R. F. Davis & K. Kobashi, J. Crys. Growth, **99**, 1168-76 (1990).

9. J. S. Ma, H. Kawarada, T. Yonehara, J. I. Suzuki, J. Wei, Y. Yokota, H. Mori, H. Fujita & A. Hiraki, Appl. Surf. Sci., **41/42**, 572-579 (1989).

10. J. S. Ma, Studies on the control of nucleation and crystal growth of CVD diamond (Osaka University, Japan, 1990).

11. G.-H. M. Ma, Y. H. Lee & J. T. Glass, J. Mater. Res., **5**, 2367-77 (1990).

12. W. Zhu, X. H. Wang, B. R. Stoner, G. H. M. Ma, H. S. Kong, M. W. H. Braun & J. T. Glass, Phys. Rev. B, **47**, 6529-6542 (1993).

13. D. Shechtman, J. L. Hutchinson, L. H. Robins, E. N. Farabaugh & A. Feldman, J. Mater. Res., **8**, 473-479 (1993).

14. B. E. Williams, H. S. Kong & J. T. Glass, J. Mater. Res., **5**, 801 (1990).

15. G.-H. Ma, Y. Hirose, S. Amanuma, M. McClure, J. T. Prater & J. T. Glass, Microstructural studies by TEM of diamond films grown by combustion flame 587 (Materials Research Society, Pittsburgh, PA, 1991).

16. G.-H. M. Ma, Microstructural Characterization of Diamond Films (North Carolina State University, 1991).

17. R. E. Clausing, L. Heatherly, K. L. More & G. M. Begun, Surf. Coat. Techno., **39/40**, 199 (1989).

18. J. L. Kaae, P. K. Gantzel, J. Chin & W. P. West, J. Mater. Res., **5**, 1480-1489 (1990).

19. A. V. Hetherington, C. J. H. Wort & P. Southworth, J. Mater. Res., **5**, 1591-4 (1990).

20. A. B. Harker & J. F. DeNatale, Journal of Materials Research, **5**, 818-823 (1990).

21. P. J. Fallon & L. M. Brown, Diamond and Related Materials, **2**, 1004-1011 (1993).

22. R. J. Graham, T. D. Moustakas & M. M. Disko, J. Appl. Phys., **69**, 3212-3218 (1991).

23. A. T. Collins, Diamond and Related Materials, 457-469 (1992).

24. R. J. Graham, J. B. Posthill, R. A. Rudder & R. J. Markunas, Appl. Phys. Lett, **59**, 2463-2465 (1991).

25. R. J. Graham, Mat. Res. Soc. Symp. Proc., **242**, 97-107 (1992).

26. R. J. Graham & K. V. Ravi, Appl. Phys. Lett., **60**, 1310-1312 (1992).

27. B. R. Stoner, G.-H. M. Ma, S. D. Wolter & J. T. Glass, Phys. Rev. B, 11067 (1992).

28. C. H. Carter, R. F. Davis & S. R. Nutt, J. Mater. Res., **1**, 811 (1986).

29. D. A. Tucker, F. R. Sivazlian, S. P. Bozeman, J. T. Glass, D.-K. Seo, M.-H. Whangbo, B. R. Stoner, A. T. Sowers & R. J. Nemanich, submitted to Surface Science, (1995).

30. J. W. Edington, **Practical Electron Microscopy in Materials Science** 1-344 (Tech Books, 1976).

31. D. A. Porter & K. E. Easterling, **Phase Transformations in Metals and Alloys** (van Nostrand Reinhold, New York, 1988).

32. D. A. Smith & W. Krakow, Mat. Res. Soc. Symp. Proc., **83**, 349-353 (1987).

33. B. R. Stoner, C.-T. Kao, D. M. Malta & R. C. Glass, Applied Physics Letters, **62**, 2347 (1993).

34. V. S. Vavilov, A. A. Gippius, A. M. Zaltsev, B. V. Deryagin, B. V. Spitsyn & A. E. Aleksenkoz, Sov. Phys. Semicond., **14**, 1078-1079 (1980).

35. L. H. Robins, L. P. Cook, E. N. Farabaugh & A. Feldman, Phys. Rev. B, **39**, 13367 (1989).

Figure Captions

Figure 1a. Diffraction pattern showing the SiC interface between the diamond and silicon.

Figure 1b. Schematic of the diffraction pattern shown in figure 1a.

Figure 2. HRTEM image of the diamond / silicon interface showing pockets of crystalline SiC.

Figure 3. HRTEM interface showing pockets of crystalline SiC and highly defective SiC between diamond and silicon.

Figure 4a. Diamond in direct contact with the silicon.

Figure 4b. A schematic showing diamond in direct contact with silicon at several different angles.

Figure 5a. Grain boundary between two grains shown in cross-section.

Figure 5b. Schematic of the grain boundary shown in figure 5a.

Figure 6. SEM of the surface of the highly oriented diamond film showing the alignment and misalignment of the diamond grains.

Figure 7. Plan view TEM micrograph of a highly oriented diamond film, the majority of the boundaries are along the <110> direction.

Figure 8. Plan view TEM micrograph of a highly oriented diamond film showing boundaries along both the <110> and <100> directions.

Figure 9. Low angle grain boundary of a highly oriented diamond films showing a series of parallel dislocations. Inset shows a diffraction pattern from the grain boundary of these two films.

Figure 10. A ball and stick model showing a 15 degree misorientation between the two grains. With this large angular misorientation, only one dislocation is observed in the model.

Figure 11a. CL spectra taken from the entire film surface.

Figure 11b. An enlargement of the area of interest at a wavelength of 433nm.

Figure 12a. CL imaging at a wavelength of 433 nm.

Figure 12b. An enlargement of the area of interest at a wavelength of 433nm.

Figure 13. TEM image corresponding to the area shown in figure 12.

Figure 14. TEM image of an apparent low angle grain boundary region.

Figure 15. CL image corresponding to the TEM micrograph in figure 14.

Figure 1a. Diffraction pattern showing silicon carbide epitaxial to silicon. Also shown, diamond grains with an offset of approximately 6 degrees with respect to the silicon and silicon carbide.

Figure 1b. Schematic of silicon/silicon carbide/diamond diffraction pattern.

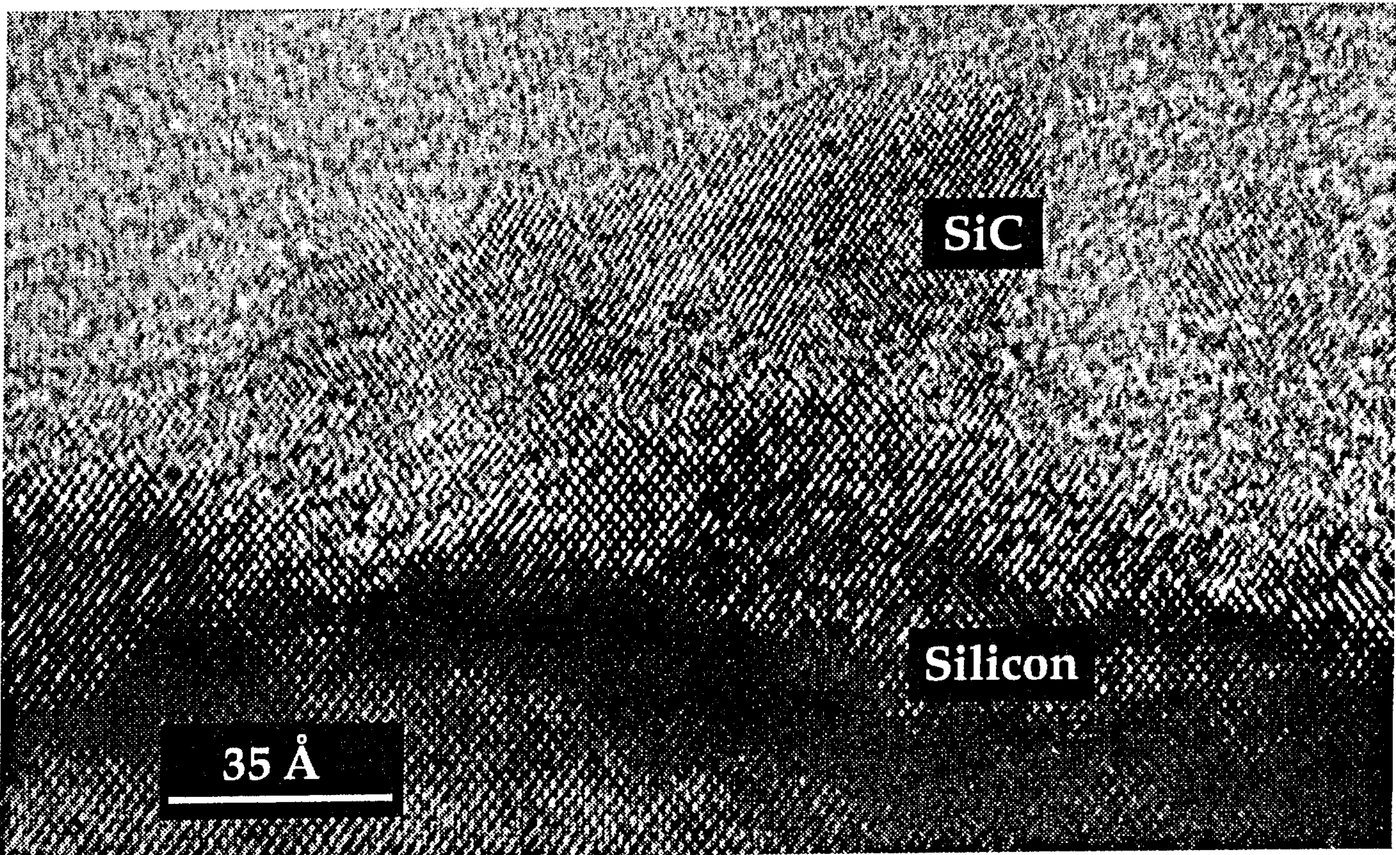

Figure 2. HRTEM of the diamond/silicon interface showing regions of crystalline SiC.

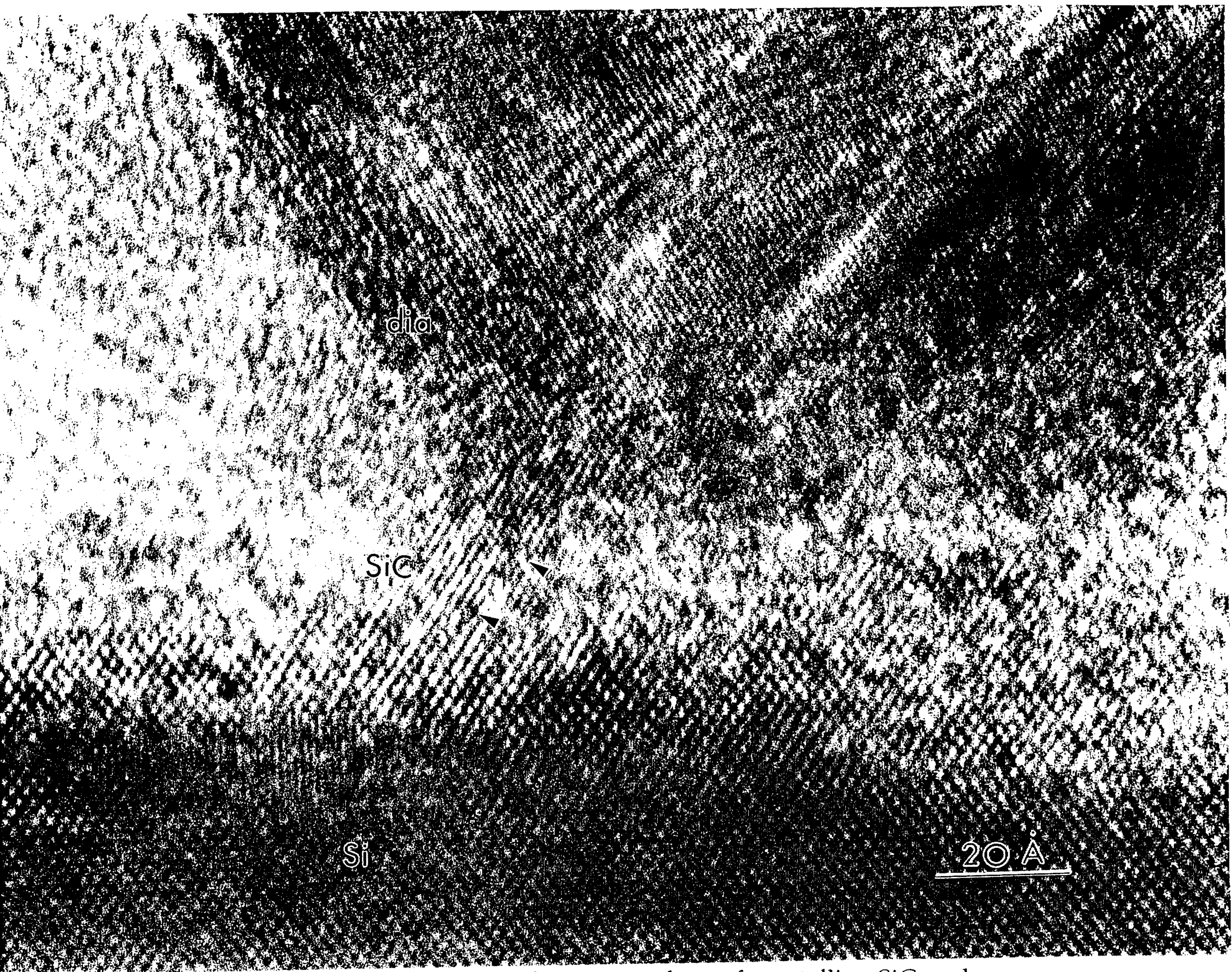

Figure 3. HRTEM interface showing pockets of crystalline SiC and highly defective SiC between diamond and silicon.

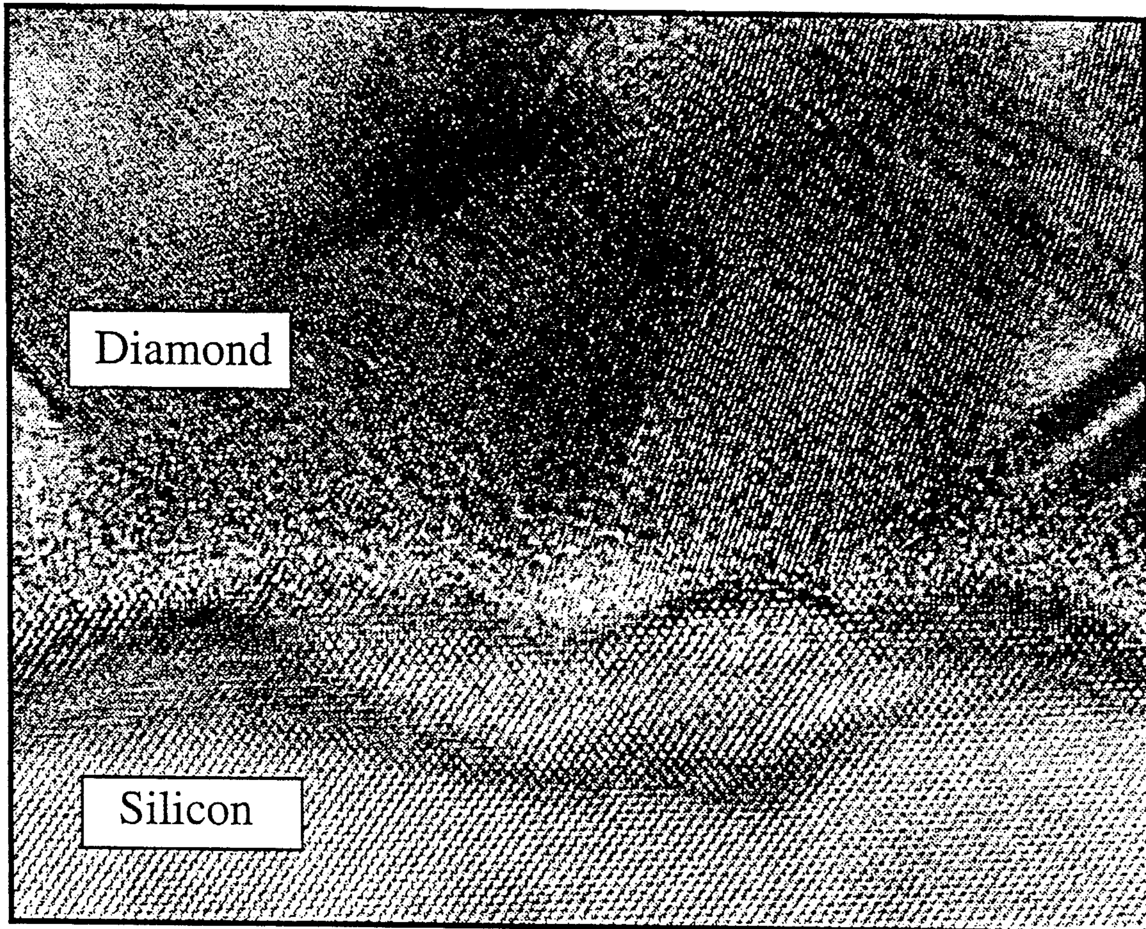

Figure 4a. HRTEM of diamond/silicon interface. The diamond and silicon are epitaxial with a 14° relationship. There is no evidence of an interlayer in this region.

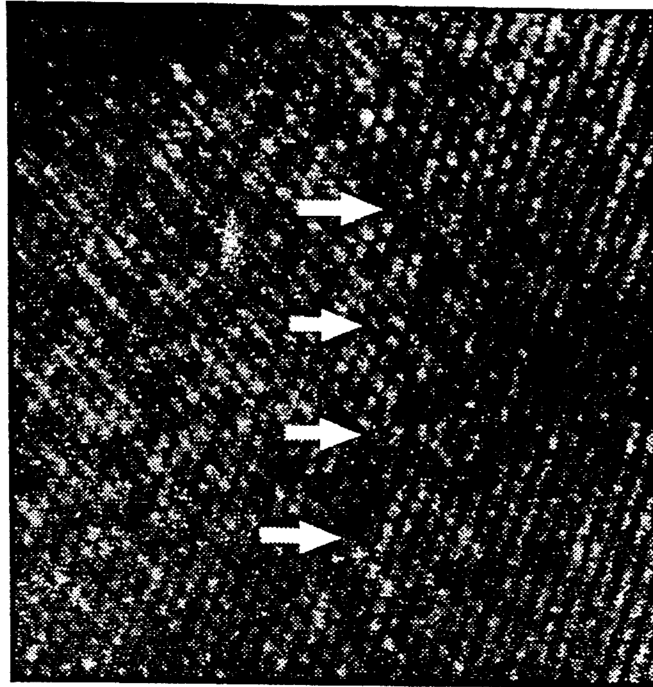

Figure 5a. Cross-sectional HRTEM micrograpgh of grain boundary. The two grains are misoriented 10° with respect to each other.

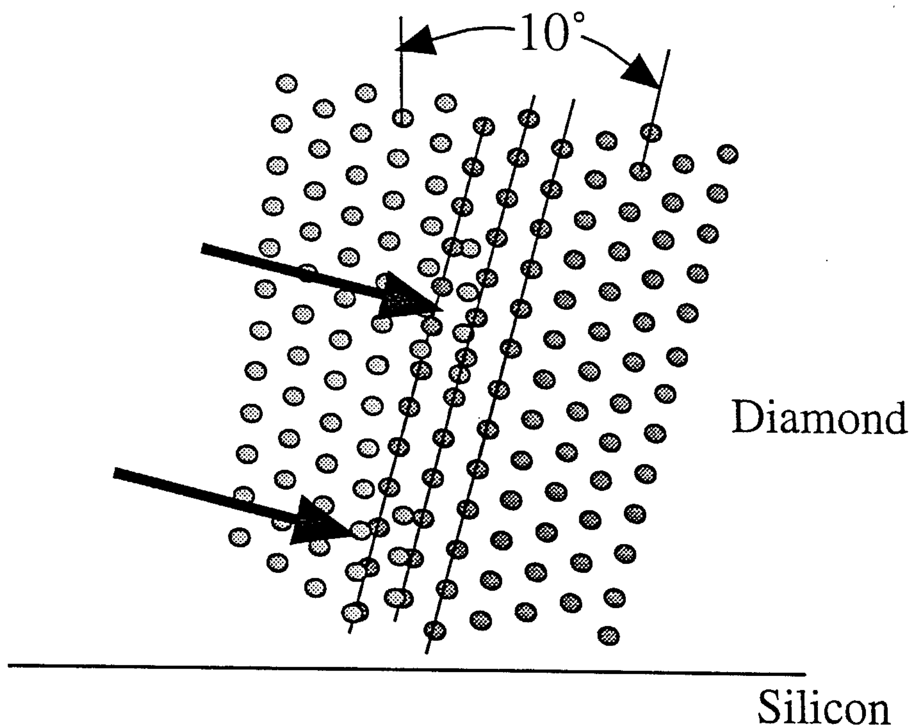

Figure 5b. A schematic of the above misorientation, areas of disorder are indicated by the arrows.

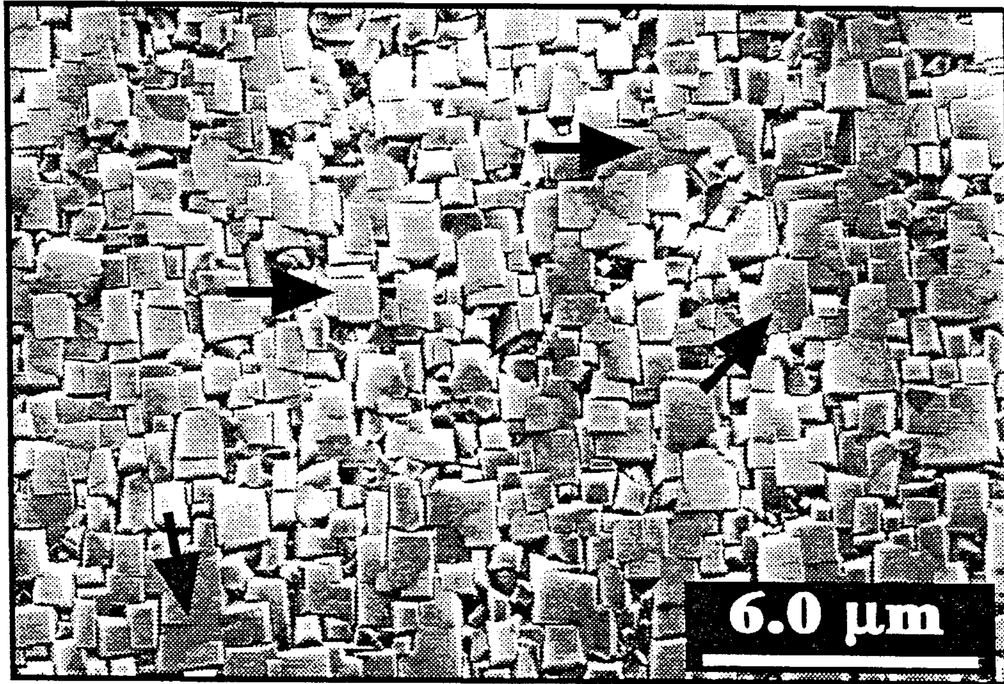

Figure 6. SEM of a highly oriented diamond film. Arrows indicate some areas where the diamond appears to have grown together.

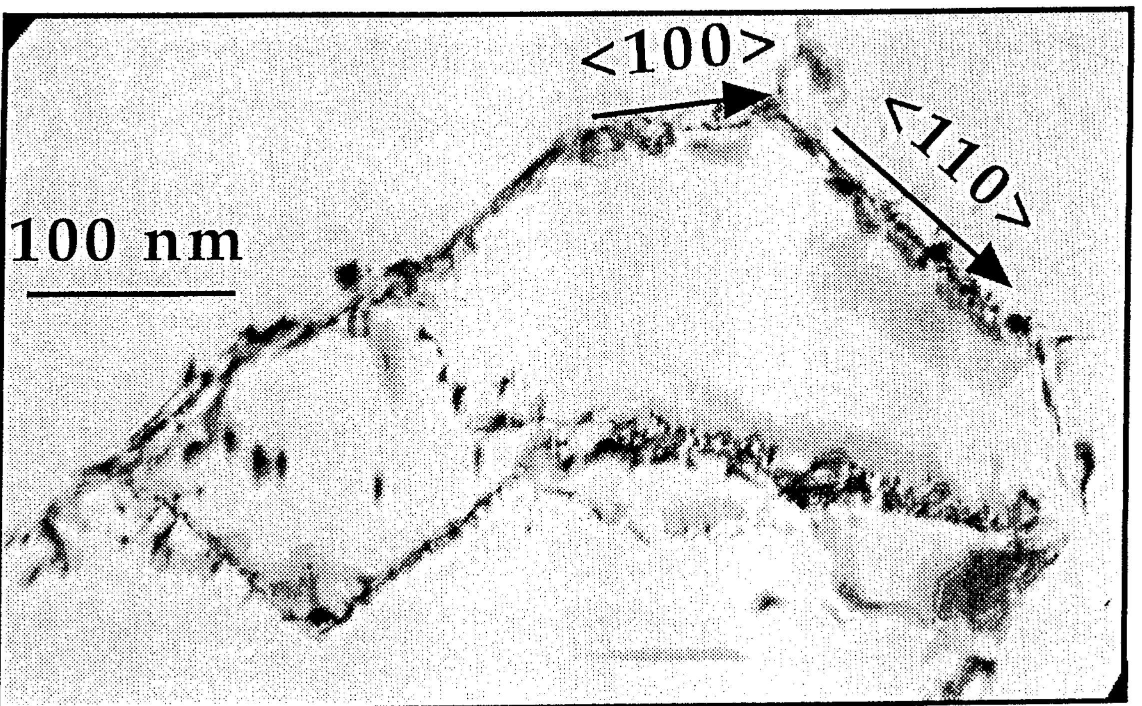

Figure 7. TEM micrograph from a highly oriented diamond film. Both <100> and <110> type boundaries are apparent.

Figure 8. TEM micrograph of a large are of the diamond film. This shows that the majority of the boundaries are along the <110> direction.

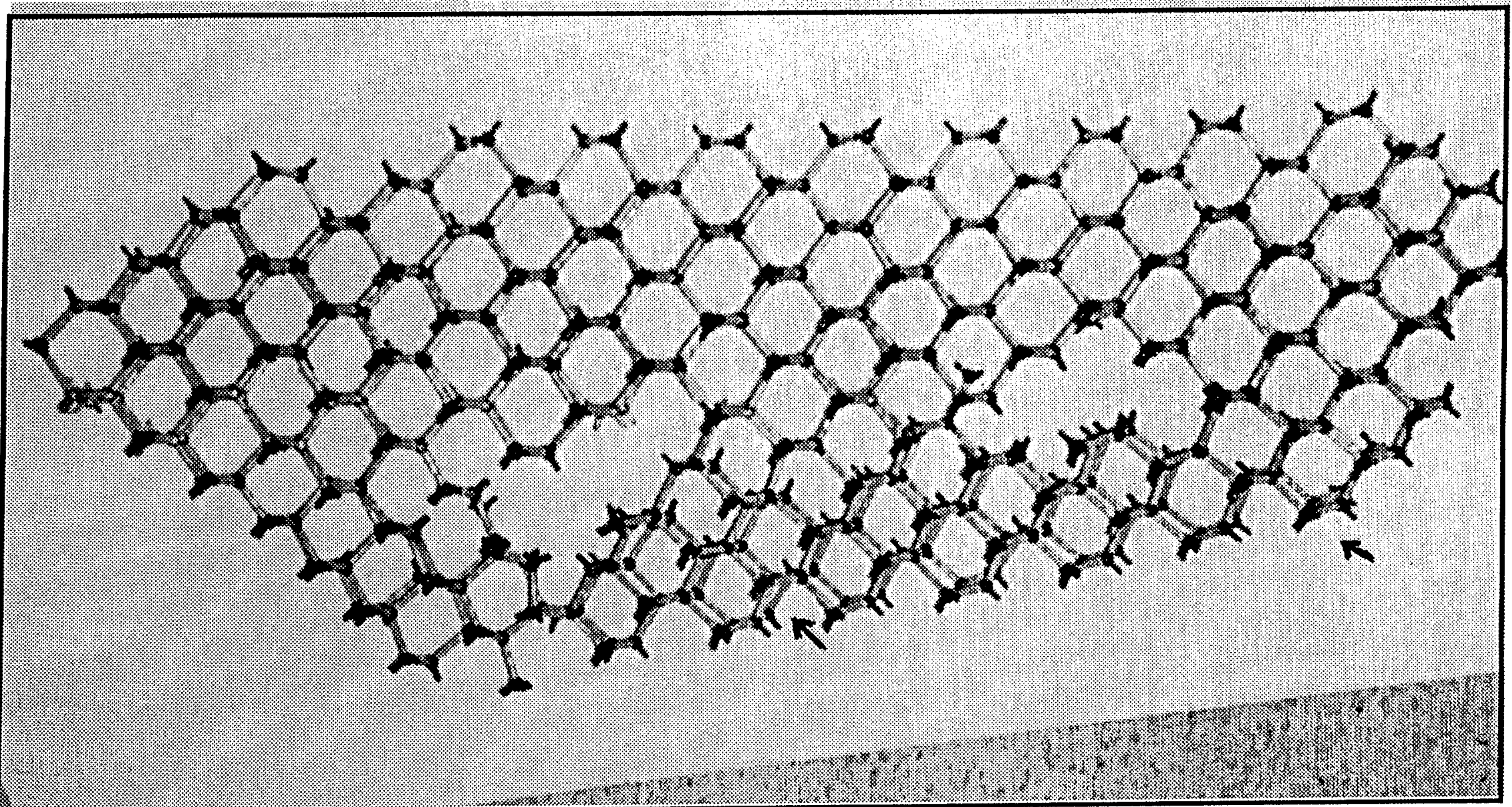

Figure 10. Model of a low angle grain boundary. Arrows indicate the extra planes of atoms.

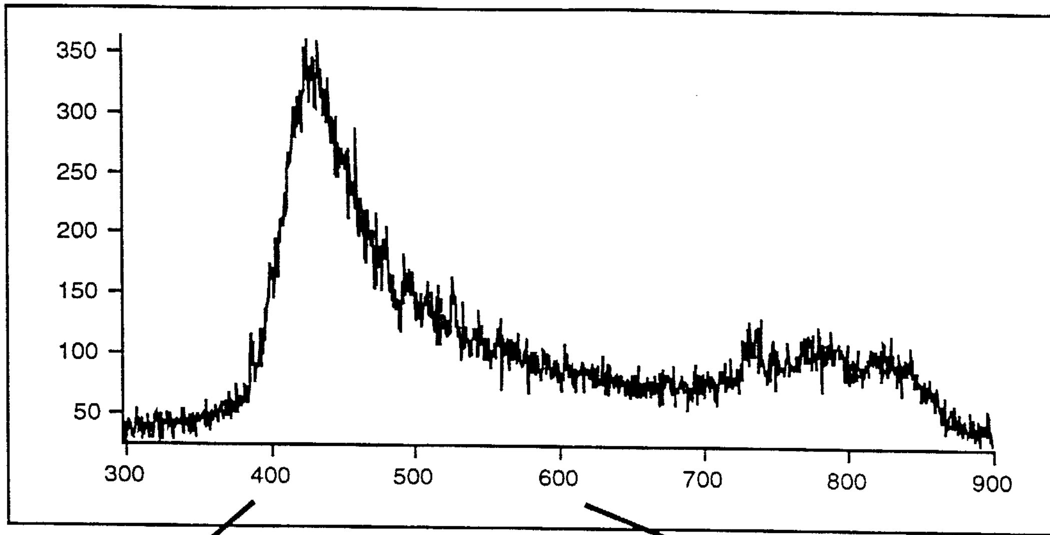

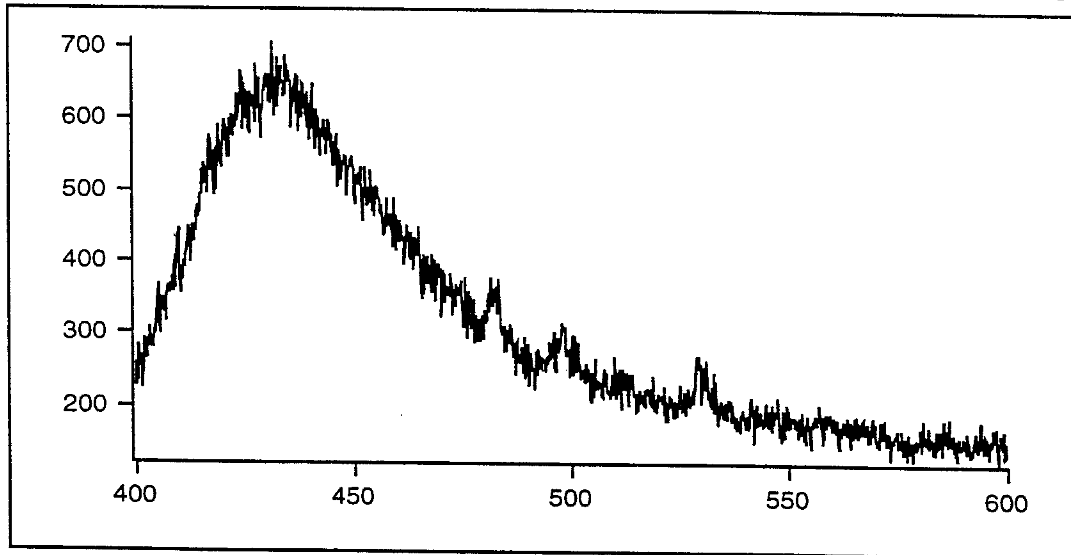

Figure 11. upper) CL spectra from a highly oriented diamond film. lower) Enlargement of Band A region, 400-600nm, which has been associated with defects in CVD diamond

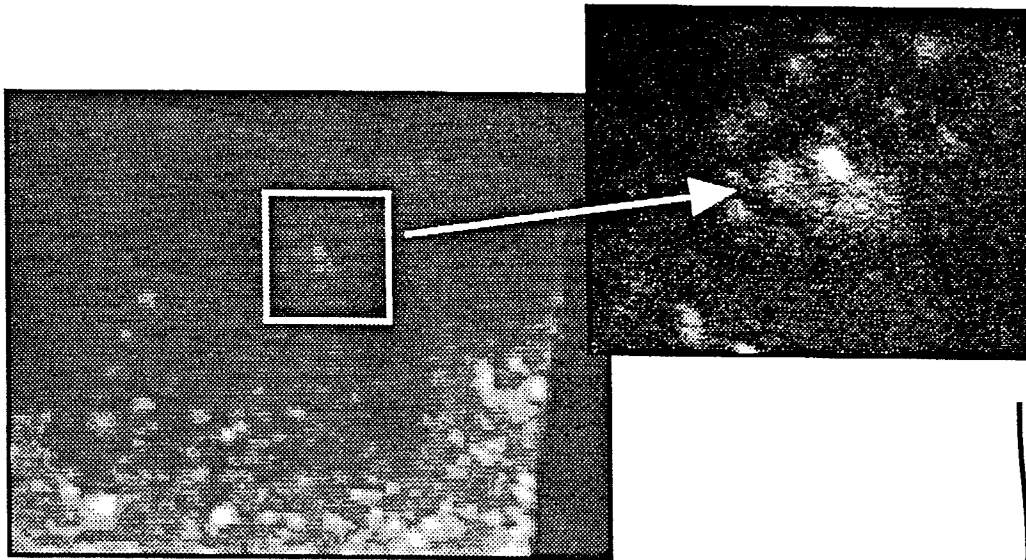

Figure 12a. CL image corresponding to the spectra in figure 11, 431nm.
12b) Enlagement of the a highly defective region.

Figure 13. TEM image of the above region, shows a highly defective region.

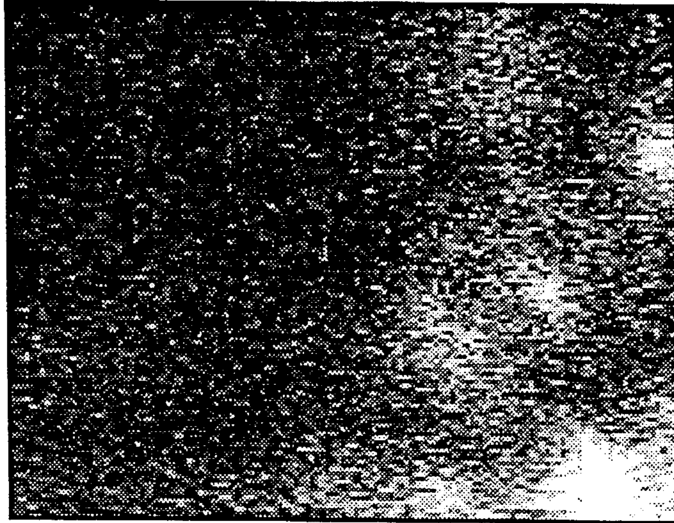

Figure 14. CL image at 433nm of a 4 grain boundary region. Luminescent area corresponds to a highly twinned region.

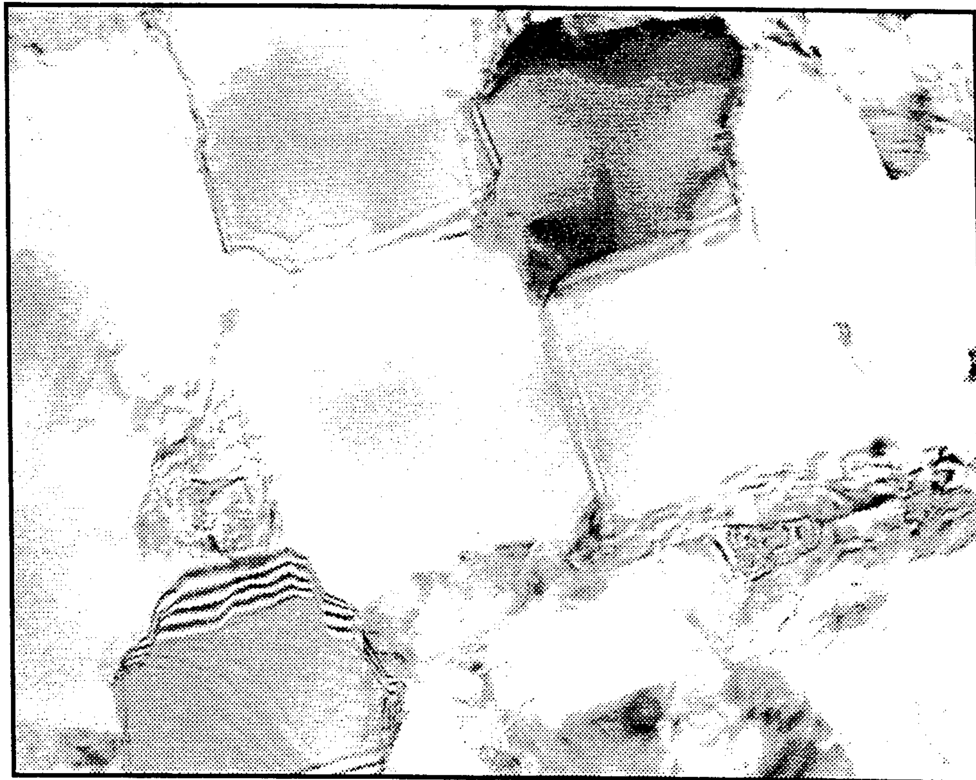

Figure 15. TEM micrograph of the region shown in figure 14.

III. Growth and Characterization of Cubic Boron Nitride Thin Films

A. Introduction

Boron nitride, like carbon, forms with three crystalline structures: a layered hexagonal form (h-BN) which is similar to graphite; cubic boron nitride (c-BN) which corresponds to diamond; and a rarer form, wurtzitic boron nitride (w-BN), which is analogous to Lonsdaleite. The last two phases are metastable at moderate temperatures and pressures.

The interest in c-BN films stems from their potential applications as hard coatings and from their electronic and thermal properties. Cubic BN is the hardest known material other than diamond. Unlike diamond, c-BN does not react with ferrous metals, and it can be used at higher temperatures before the onset of structural transformation. These properties make it an excellent cutting tool material. Bulk c-BN crystals formed using high temperature-high pressure techniques are already used in the cutting tool industry. Electronic applications of cubic boron nitride would take advantage of its very wide band gap ($E_g \approx 6.4$ eV [1]), its ability to be doped both p-type and n-type with Be and Si, respectively [2], and for some applications its very high thermal conductivity.

Cubic boron nitride was first grown in bulk crystal form in 1956 [3]. Reports of c-BN in thin film form appeared as early as 1970 [4], but it was not until about 1987 that thin films conclusively characterized as cubic boron nitride were achieved [5]. Subsequently, many groups have successfully grown c-BN using various techniques including ion beam assisted deposition [6,7] r.f. sputtering [8], ion plating [9], laser ablation [10,11], ECR plasma [12], and chemical vapor deposition (CVD) [13].

Cracking and loss of adhesion of deposited c-BN films are frequently reported phenomena, which have been attributed to a high level of intrinsic compressive stress in the films [14,15]. Murakawa [9] has attempted to overcome this problem using buffer layers between the substrate and the BN film, including a graded B to BN layer and a TiN layer, together with post-deposition annealing of the films. Okamoto *et al.* [16] also used a graded B to BN buffer layer in CVD c-BN films. Both studies produced well adhered films. No reports have appeared of stress-free c-BN films grown directly on a substrate. By contrast, recent research strongly indicates that a high stress level in the film is a necessary condition for the formation of the cubic phase [15, 17].

An additional challenge is growing epitaxial films, which would be essential for the majority of electronic device applications. No reports of reproducible experiments of epitaxial growth of c-BN have appeared. A better understanding of what happens at the substrate-BN interface needs to be developed. In a previous paper [17] we have shown that when BN is deposited on Si, initial amorphous and hexagonal BN layers grow before cubic

growth begins. If these interfacial layers are necessary precursors to c-BN growth, then it would appear exceedingly challenging to grow epitaxial c-BN using current PVD methods.

An area of research where significant progress has been made is in determining the deposition conditions necessary for c-BN growth. The work of Kester and Messier [18] established that for a given substrate temperature, the momentum transferred into the growing film by the bombarding ions is the single parameter which controls the formation of c-BN. As long as sufficient N is present, a threshold value of momentum transfer exists for the formation of c-BN. This controlling parameter incorporates the values of ion energy, ion flux, and ion species. As a result of the present study described below we have developed a better understanding of both the conditions required for c-BN growth and of the mechanisms responsible for that growth.

B. Experiment

Deposition. Ion beam assisted deposition (IBAD) has been used successfully for c-BN growth [17,18]. It is particularly useful in that the B deposition rate, bombarding ion energy, ion flux and ion species can be controlled and measured independently. This allows for good quantification of the deposition process. The IBAD configuration in the present study employed electron beam evaporation of boron together with simultaneous bombardment by nitrogen and argon ions from a Kaufman ion source. A schematic of the deposition system is shown in Fig. 1.

The substrates used in this study were (100) single crystal infrared-transparent, high resistivity (ρ>50 Ω-cm) on-axis Si; cut and polished single crystal natural diamond; as well as polished single crystal Cu and Ni. The Si substrates were cleaned using a standard RCA procedure [19] of which the final step was a 5 min dip in 10% HF. This left the surface H terminated, as determined by XPS. The diamond substrates were etched in a boiling 3:4:1 H_2SO_4:HNO_3:$HClO_4$ solution for 45 minutes to remove any graphitic phase, and the Cu and Ni substrates were decreased ultrasonically in a sequence of TCE, acetone, methanol, and DI water. The substrates were attached to Mo holders using Ag paint which acted both as an adhesive and a thermal conductor. This assembly was subsequently loaded through a vacuum load lock into the UHV deposition chamber. Base pressures in the chamber were typically 5-8 $\times$ 10^{-10} Torr.

Each substrate was heated using a W wire coil located behind the Mo substrate holder. They were baked under UHV conditions at 700°C for 20 min to remove residual H_2O and hydrocarbon species. The substrate temperature during deposition was monitored using thermocouples near the heater, the readings of which had been previously calibrated to several temperatures of the substrate surface. Boron was deposited using a constant deposition rate of 0.5 Å/s, which was monitored using a quartz crystal rate monitor. Fluxes of

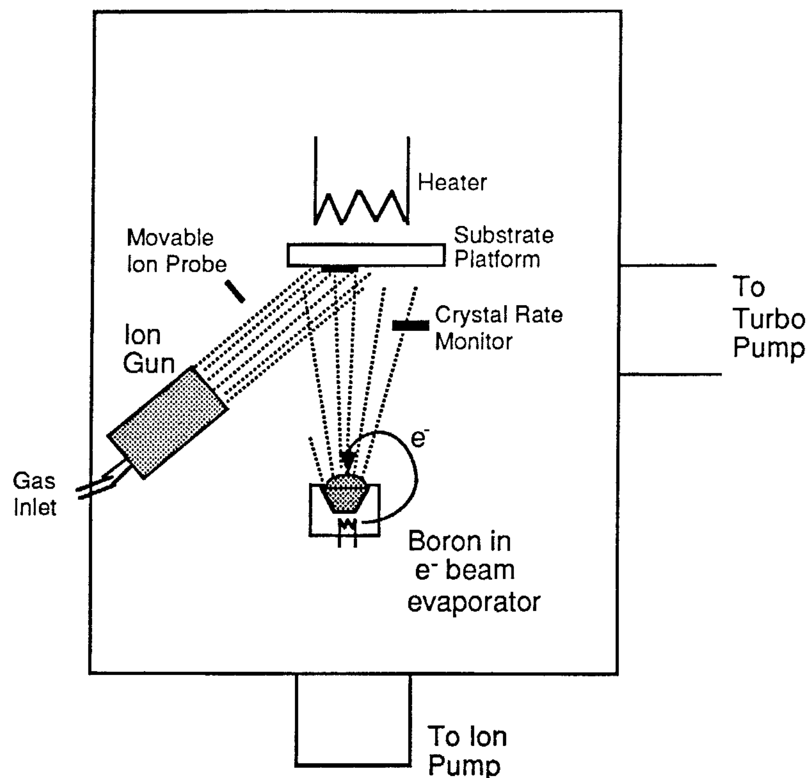

Figure 1. Schematic of UHV electron beam evaporator-based IBAD system used in this research.

N and Ar ions were obtained from a 3 cm Ion Tech Kaufman source. Argon and nitrogen gases were used with a gas flow ratio of 1:1. Because of the close ionization potentials of these two gases, the ion ratio was also close to 1:1. The ion source was operated at 500 eV; based on the studies of Hubler *et al.* [20] the N ions were predominantly N_2^+. The discharge voltage of this source was maintained at a sufficiently low value to prevent double ionization of either species. Since it has been previously shown that c-BN can be successfully deposited using an Ar:N_2 ratio of 1:1 and an ion energy of 500 eV [17,18], these values were maintained constant throughout this study.

Both the ion beam and the boron evaporation were started and allowed to stabilize before deposition. During this period, the substrate was covered by a movable shutter. To eliminate the potential for surface damage, there was no pre-deposition ion bombardment of the substrates.

Characterization methods. The primary method of film characterization was Fourier transform infrared spectroscopy (FTIR) due to the ability to distinguish between the cubic and hexagonal or amorphous forms of BN. Cubic BN has a transverse optical mode absorption peak at 1075 cm^{-1}, while amorphous and hexagonal BN have a primary absorption peak at 1367 cm^{-1} and a secondary peak at 783 cm^{-1} [21,22]. The spectra were obtained using an Analect Instruments model fx-6260 spectrometer. The IR beam was passed through the

BN coated substrate. A ratio of the resultant spectrum to that obtained from a background scan taken from an uncoated substrate was determined. Reflectance FTIR was employed to characterize the films deposited on the IR opaque Cu and Ni substrates. The latter study was conducted on a Nicolet 620 FTIR equipped with a Spectra Tech IR Plan optical microscope.

The film crystallography and the film-substrate interface were studied via high resolution cross sectional transmission electron microscopy (HRTEM) using a JEOL 4000EX operated at 400kV. The images were recorded using a 1mr convergence semi-angle at a Scherzer defocus of ~ 47nm. Samples were prepared using standard techniques [23].

Rutherford backscattering spectrometry (RBS) was used to measure the compositions and thicknesses of the films due to this techniques ability to give a depth profile of the film, not only information about the surface layer. 2.0 MeV primary He^+ ions and a 165° scattering angle were used for measuring the energy of the backscattered nuclei. The samples were tilted 6° to prevent channeling.

C. Results

FTIR Results. The results reported in this and the following subsection were obtained using only Si(100) substrates. To study the effect of substrate temperature (T_S) on the BN films, depositions were conducted from 200°C to 700°C. All other variables were held constant. The results of one of these series of depositions are shown in Fig. 2. There was almost no cubic phase in the 200°C film. In the temperature range of 300-400°C, the films were a mixture of the cubic and hexagonal/amorphous phases (IR does not distinguish between the hexagonal and amorphous forms of BN). The relative amount of cubic phase increased with increasing temperature. At some temperature above 400°C the amount of cubic phase began to drop rapidly; it was not observed at all in the film deposited at 700°C. These results correspond well with those of other researchers [24] who have also found that the best temperature for growing cubic boron nitride is at or close to 400°C.

A second significant parameter studied was the ion bombardment flux. As discussed above, it has been previously shown [18] that the critical parameter (at constant temperature) for growing the cubic phase is momentum, p, transferred from the bombarding ions into the growing film per deposited boron atom, p/a, where a is the boron flux measured in atoms $cm^{-2}\ s^{-1}$. This critical value is given by

$$\frac{p}{a} = \frac{J}{a}\sqrt{2m\gamma E} \qquad (1)$$

where J/a is the ratio of bombarding ions to depositing boron atoms. J is the ion flux measured in ions $cm^{-2}\ s^{-1}$, *m* is the mass of the bombarding ions and E is their energy. The maximum energy transfer from the ion to the atom, γ, is given by

$$\gamma = \frac{4mM}{(m+M)^2} \tag{2}$$

with M being equal to the average mass of the atoms being bombarded. There is a linear relationship between the ion flux, J, and the momentum transfer value. Therefore a change in the ion flux (while keeping the ion energy and ion species distribution constant) acts directly as a change in momentum transfer. Since changing the ion energy, E, has less of an effect on the momentum (momentum being proportional to the square root of the energy), the bombardment level in this study was varied by varying the ion flux and keeping the ion energy constant.

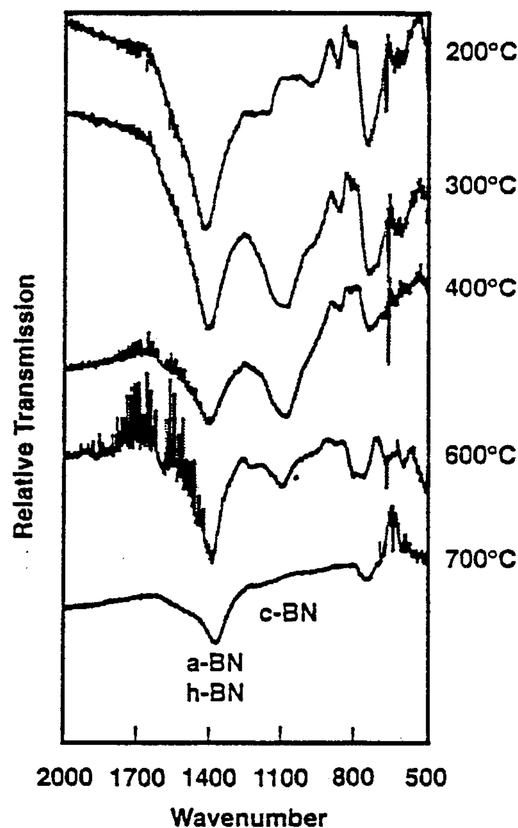

Figure 2. FTIR spectra of BN films deposited on Si(100) at various substrate temperatures. Other deposition conditions were film thickness: 200Å; ion flux: 0.32 mA/cm^2; boron deposition rate: 0.5 Å/s; ion energy: 500 eV; ion bombardment by 50:50 $Ar:N_2$.

Fig. 3(a) shows the effect of changing the ion flux while keeping the temperature constant at 600°C. Essentially no cubic phase is observed until the ion flux reaches 0.30 mA/cm^2. The small peaks observed at 1050–1100 cm-1 at the two lower flux values are due to the Si substrate. This confirms that there is a minimum momentum transfer level, and therefore ion flux, necessary to grow the cubic phase at a given temperature. The spectra shown in

Fig. 3(b) are from films grown at the same conditions as those in Fig. 3(a), except at 400°C. There is a small cubic peak visible at 0.20 mA/cm^2, and the films are predominantly cubic at 0.24 and 0.30 mA/cm^2. Comparing Figs. 3(a) and (b) confirms the result seen in Fig. 2 that increasing the substrate temperature above 400°C lowers the proportion of cubic phase in the film.

The data presented above indicated that increasing the ion flux, and thereby the momentum transfer, increases the amount of cubic phase in a film, and that increasing the substrate temperature above 400°C decreases the proportion of cubic phase. However, our previous FTIR and HRTEM results [17] showed that the relative amount of each phase in a 400°C film was also a function of film thickness. These films contained very thin amorphous and hexagonal layers of essentially constant thickness prior to the nucleation and growth of the c-BN layer. Nucleation of the pure cubic phase did not occur until a specific total thickness of the non-cubic phases was achieved.

As such, the FTIR spectra of films of different thicknesses deposited under identical conditions showed that the thicker films had a higher cubic to non-cubic ratio. Examination of films of different thicknesses prepared using the conditions of the 200Å thick 700°C film of Fig. 2, showed the same effect, as demonstrated in Fig. 4. The 100Å film and the 200Å films were completely amorphous/hexagonal, but the 400Å film was predominantly cubic. Similarly, FTIR of a set of films of different thicknesses prepared under the same conditions as the 600°C film of Fig. 2, revealed a growth sequence and layer thicknesses of non-cubic (<200Å), partially cubic (200Å), and predominantly cubic (remainder of film). These results indicate (and the HRTEM results noted below prove) that the different proportions of amorphous/hexagonal and cubic phase found in the different films are not due to different amounts of each phase interspersed through the film, but rather to the transition from single phase hexagonal to single phase cubic occurring at varying thicknesses depending on growth conditions. Specifically, the differences between the 400°C, 600°C, and 700°C films seen in Fig. 2, which ranged from significantly cubic at 400°C to completely non-cubic at 700°C are due to varying thicknesses at which the growth of the cubic phase layer begins. A higher substrate temperature delays the onset of the cubic phase. Increased ion flux enhances the onset of this phase.

HRTEM results. High resolution TEM images of films deposited at 200°C, 400°C, and 700°C are shown in Figures 5(a), 5(b), and 5(c). The film deposited at 200°C (Fig. 5(a)) has a 70Å amorphous layer at the Si interface followed by a layer of oriented h-BN. No c-BN is present. The film deposited at 400°C (Fig. 5(b)) has a 20Å amorphous layer followed by 50Å of oriented h-BN followed by c-BN. The film grown at 700°C (Fig. 5(c)) has a 50Å amorphous layer followed by a ~150Å layer of predominantly partially oriented h-BN material with a small amount of c-BN, followed by a c-BN layer.

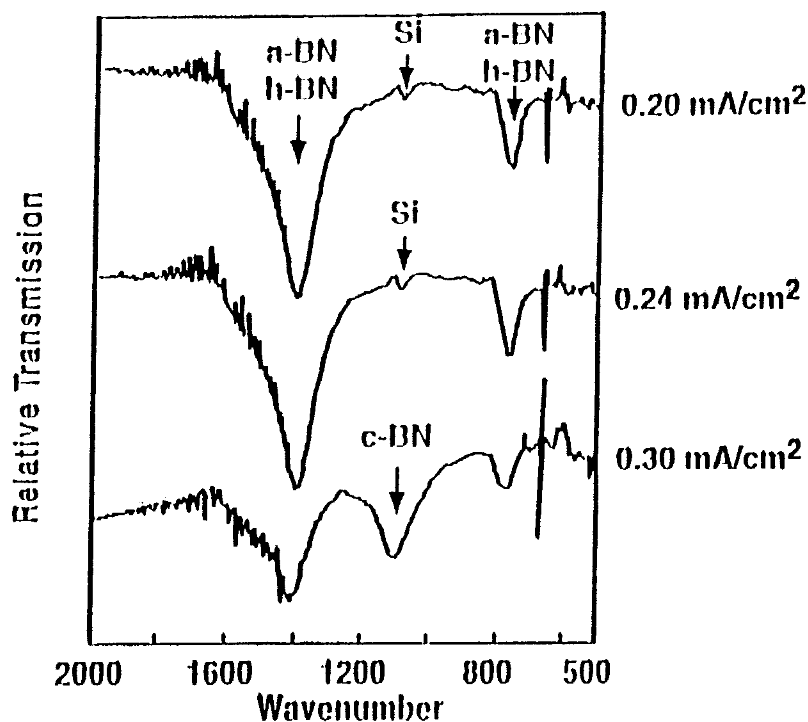

Figure 3 (a). FTIR spectra of a BN film deposited on Si(100) with various ion bombardment fluxes at a substrate temperatures of 600°C. Other deposition conditions were film thickness: 250Å; boron deposition rate: 0.5 Å/s; ion energy: 500 eV; ion bombardment by 50:50 $Ar:N_2$.

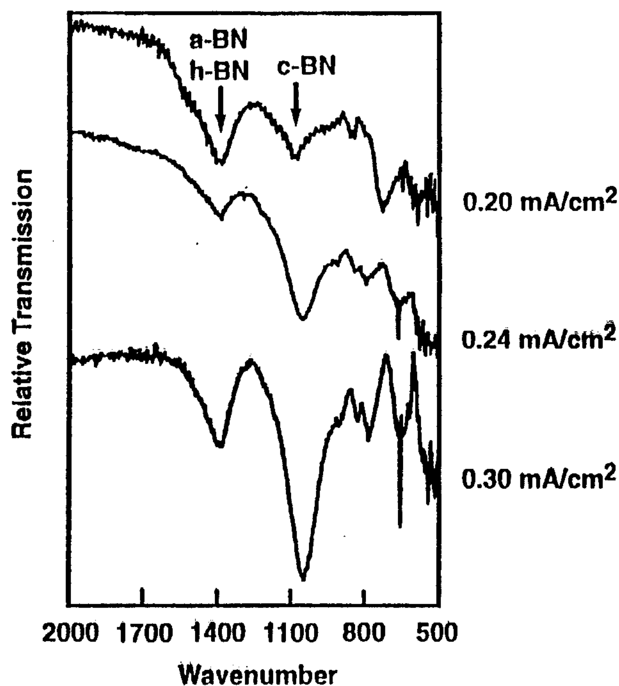

Figure 3 (b). FTIR spectra of a BN film deposited on Si(100) with various ion bombardment fluxes at a substrate temperatures of 400°C. Other deposition conditions were film thickness: 250Å; boron deposition rate: 0.5 Å/s; ion energy: 500 eV; ion bombardment by 50:50 $Ar:N_2$.

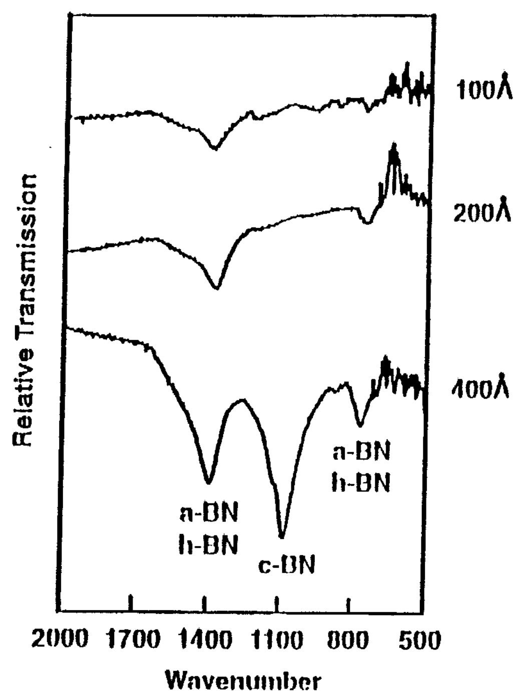

Figure 4. FTIR spectra of BN films deposited on Si(100) with various thicknesses. Other deposition conditions were substrate temperature: 700°C; ion flux: 0.32 mA/cm^2; boron deposition rate: 0.5 Å/s; ion energy: 500 eV; ion bombardment by 50:50 Ar:N_2.

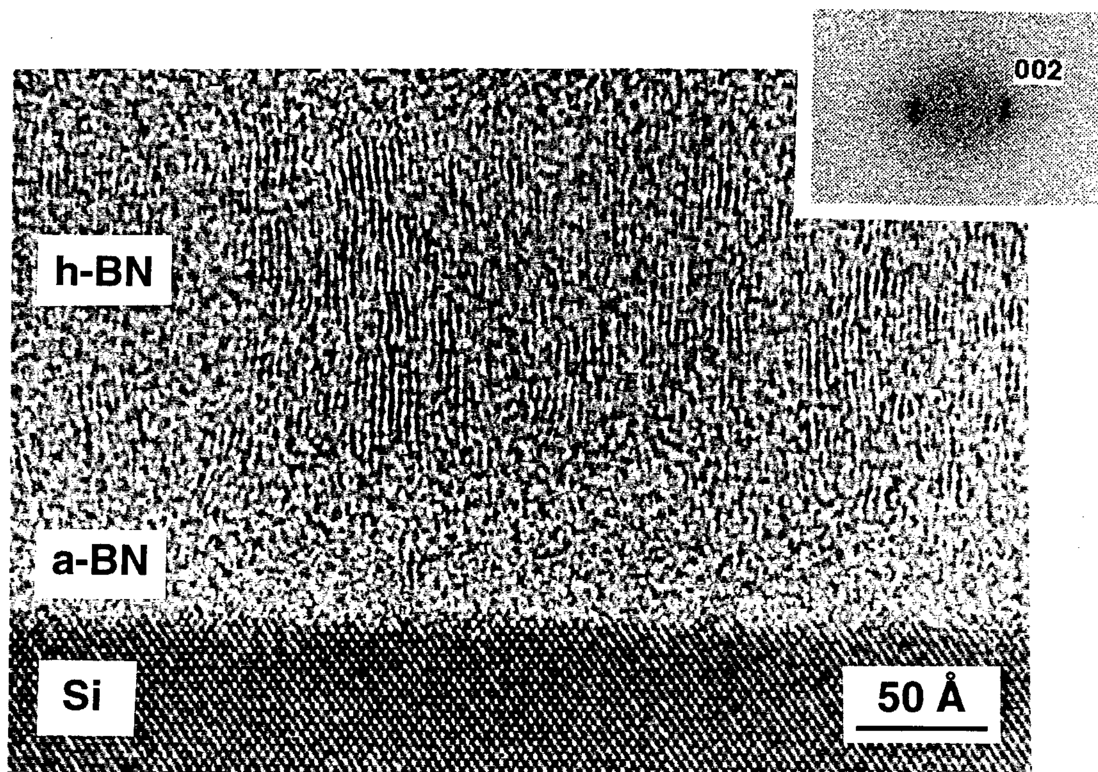

Figure 5(a). HRTEM image of a film deposited on Si(100) at 200°C. Other deposition conditions were ion flux: 0.28 mA/cm^2; boron deposition rate: 0.5 Å/s; ion energy: 500 eV; ion bombardment by 50: 50 Ar:N_2.

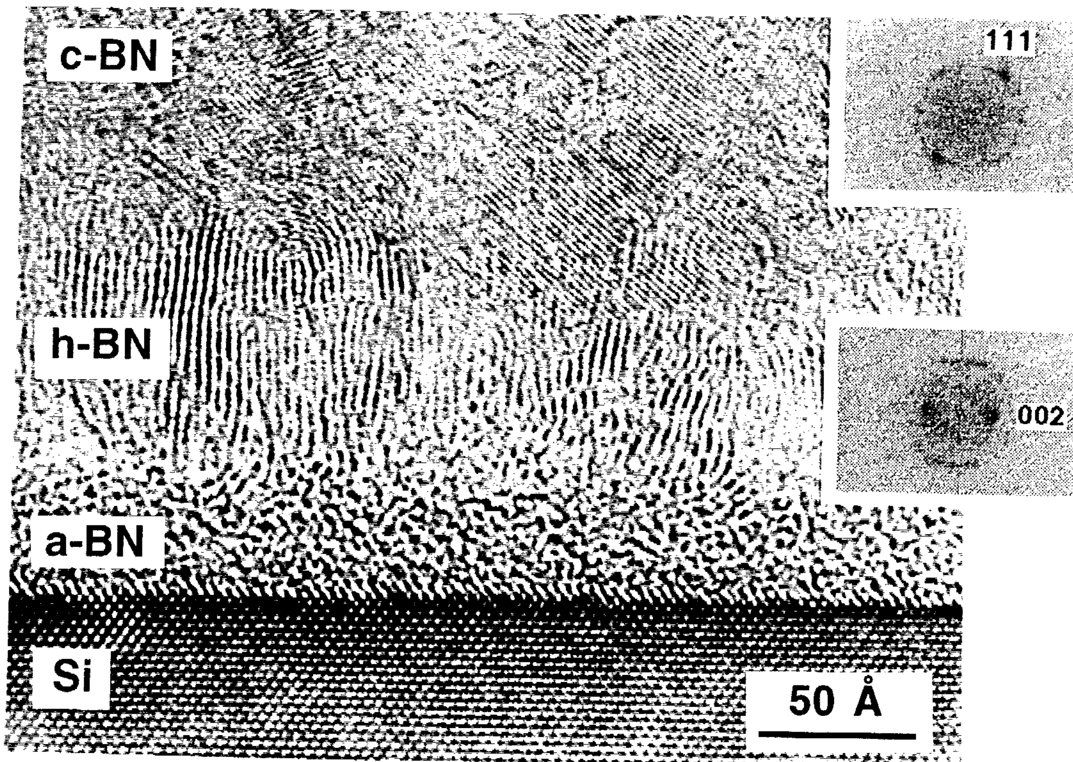

Figure 5(b). HRTEM image of a film deposited on Si(100) at 400°C. Other deposition conditions were ion flux: 0.12 mA/cm^2; boron deposition rate: 0.25 Å/s; ion energy: 500 eV; ion bombardment by 50: 50 Ar:N_2.

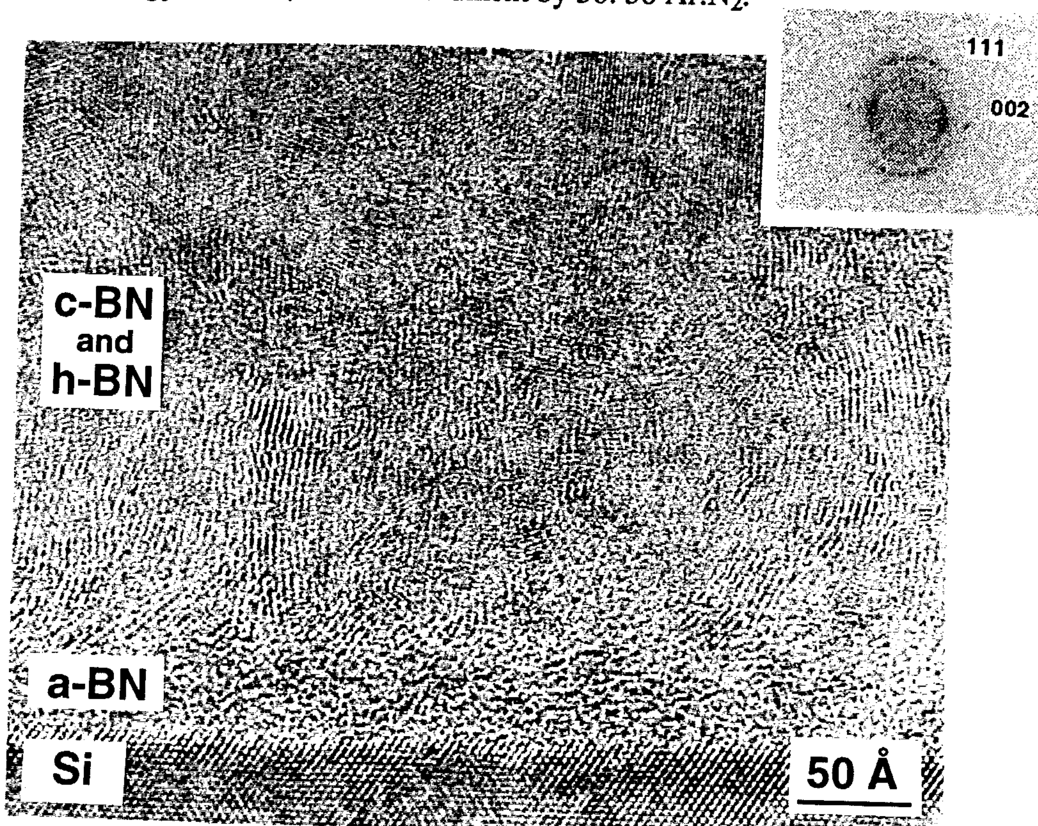

Figure 5(c). HRTEM image of a film deposited on Si(100) at 700°C. Other deposition conditions were ion flux: 0.28 mA/cm^2; boron deposition rate: 0.5 Å/s; ion energy: 500 eV; ion bombardment by 50: 50 Ar:N_2.

RBS Results. The BN grown for RBS was deposited on the lower atomic number substrate of Be to circumvent overlap of the spectra of the Si substrate with that of the film. The deposition conditions were those which resulted in c-BN growth on Si: a substrate temperature of 400°C, ion energy of 500eV, and an ion flux of 0.24 mA/cm^2. The film thickness was 500Å. The results are shown in Fig. 6. Rutherford backscattering is more sensitive to elements of higher atomic number, due to their larger nuclear cross sections. Therefore, the sizes of the original peaks at various channel numbers do not directly show their actual concentration. Computer modeling of the spectra revealed that in addition to the expected Be, B, and N, there was O due to a BeO layer on the substrate as well as Ar, Fe, and Hf in the film having the atomic percentages of ~1.5%, ~0.2%, and ~0.05%, respectively. The Ar was derived from the ion bombardment during growth; the Fe was probably due to the ion beam bombardment of the stainless steel shutter above the substrates, and the Hf was very likely derived from resputtering of residual amounts previously deposited on the substrate block.

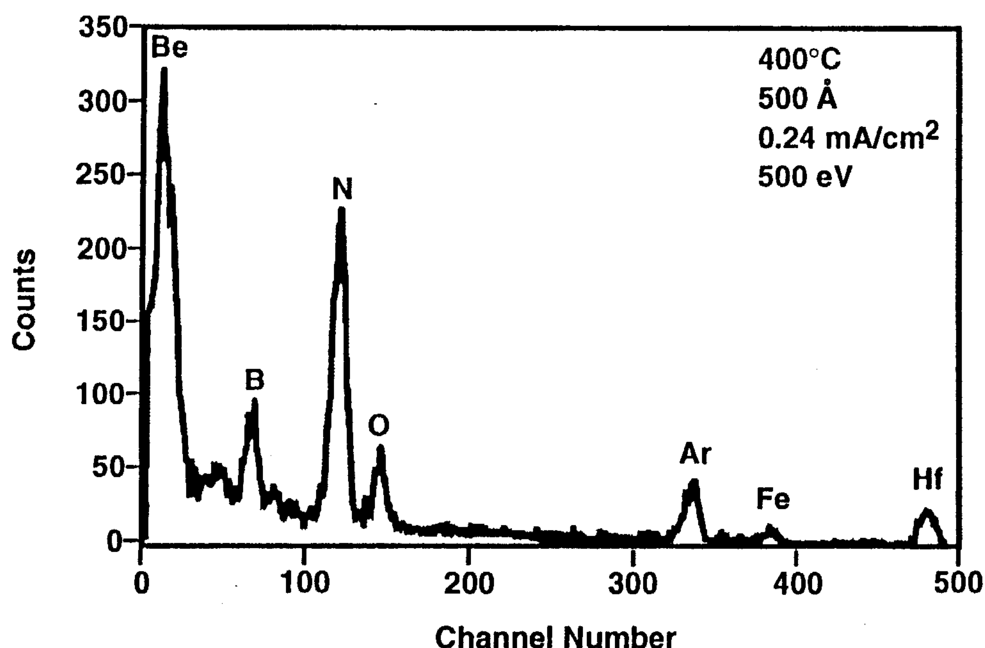

Figure 6. RBS spectra of a BN film on a beryllium substrate. Deposition conditions were film thickness: 500Å, substrate temperature: 400°C; ion flux: 0.24 mA/cm^2; boron deposition rate: 0.5 Å/s; ion energy: 500 eV; ion bombardment by 50:50 Ar:N_2.

Other Substrates. Films having a thickness of 1000 Å were grown on diamond at substrate temperatures of 400° and 600°C using an ion energy of 500eV and an ion flux of 0.24 mA/cm^2. A representative FTIR pattern of one of the films deposited at 400°C is shown in Fig. 7. A sharp c-BN peak is observed at ~1080 cm^{-1}. The h-BN peak is very small. The

spectrum of this relatively thick film has a sharper c-BN peak and a better c-BN to h-BN ratio than any of the films we had previously deposited on Si, and is as good or better than any that have previously appeared in the literature. For the film grown at 600°C the FTIR spectrum was essentially the same.

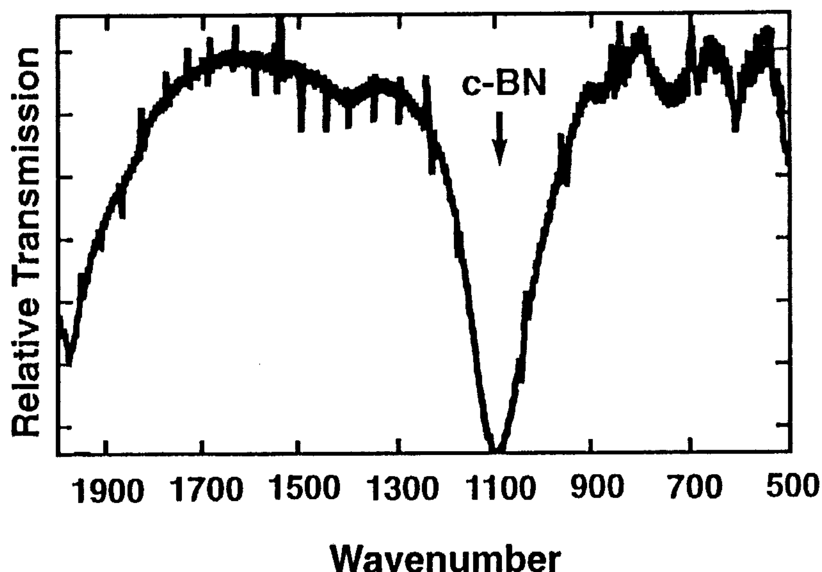

Figure 7. FTIR spectra of BN deposited on a single crystal diamond(100) substrate. Deposition conditions were film thickness: 1000Å, substrate temperature: 400°C; ion flux: 0.24 mA/cm^2; boron deposition rate: 0.5 Å/s; ion energy: 500 eV; ion bombardment by 50:50 Ar:N_2.

Observation via SEM of the films deposited at 400°C showed occasional cracking. The films deposited at 600°C showed no cracking or delamination. Films deposited under the same deposition conditions and the same thicknesses on Si exhibited both severe cracking and delamination.

High resolution TEM was performed on the sample grown at 600°C, and an image is shown in Fig. 8. The same type of layered structure observed on BN grown on Si is present, although not as pronounced.

Nickel and Cu also have lattice spacings very close to that of c-BN, with a lattice mismatch for Ni of 2.6% and for Cu of less than 0.05%. Therefore it was thought that like diamond (which has a lattice mismatch of 1.4%) they may be better substrates for c-BN growth than Si which has a lattice mismatch of 33%. Films having a thickness of 500Å were grown at 400°C under the same conditions of ion flux and ion energy employed in the deposition on diamond. As shown in Fig. 9, reflectance FTIR from films grown on the Ni

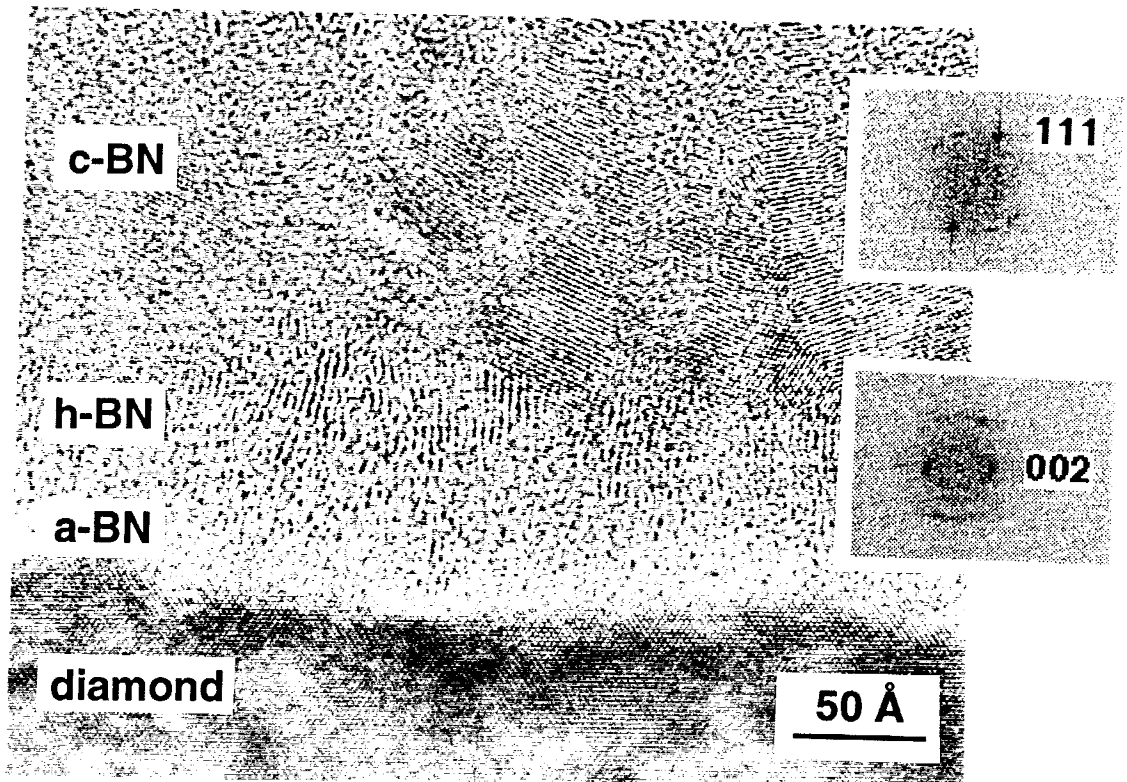

Figure 8. HRTEM image of a 600°C film on a diamond(100) substrate. Other deposition conditions were ion flux: 0.28 mA/cm^2; boron deposition rate: 0.5 Å/s; ion energy: 500 eV; ion bombardment by 50:50 Ar:N_2.

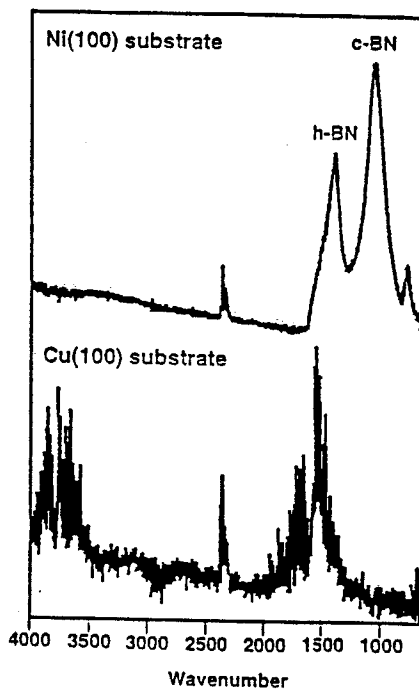

Figure 9. Reflectance FTIR of BN deposited on Cu(100) and Ni(100) substrates. Deposition conditions were film thickness: 500Å, substrate temperature: 400°C; ion flux: 0.24 mA/cm^2; boron deposition rate: 0.5 Å/s; ion energy: 500 eV; ion bombardment by 50:50 Ar:N_2.

substrate revealed a mixture of h-BN and c-BN; films grown on Cu were h-BN with no evidence of c-BN.

D. Discussion

The above results show that the onset of c-BN growth is a function of temperature, ion momentum transfer and deposition period (film thickness). McKenzie *et al.* [14,15] have shown theoretically and experimentally that the effect of deposition period is caused by the build-up of biaxial compressive stresses in the growing film. They observed by FTIR, electron energy loss spectroscopy and TEM an initial layer of h-BN oriented perpendicular to the substrate surface. The nucleation and growth of c-BN occurred as the stress in the film increased. No amorphous phase was reported. The stress at the onset of c-BN growth corresponded to conditions in the high pressure regime where this phase is stable. The present results can be understood using this model. Increasing the substrate temperature from, for example, 400°C to 700°C, results in both a higher surface mobility of the adsorbed species and possibly bulk annealing, which allow stress relaxation. Thus, as shown in Fig. 4, the higher the deposition temperature the greater the film thickness necessary to reach the stress level required for c-BN nucleation and growth, all other conditions being the same. There is a sharp increase in the transition thickness, and therefore a sharp drop in stress, within the 600-700°C temperature range. This corresponds with the results of Windischmann [25] who found in several different materials, that increasing the deposition temperature from room temperature causes a gradual decrease in the intrinsic stress , followed by a sharp drop when the temperature reaches $T_m/3$, where T_m is the melting point. For BN, $T_m/3$ is ~700°C.

The foregoing explanation does not account for the results of decreasing the temperature below 400°C, for it does not further lower the threshold thickness for initiation of the cubic phase. In fact, at these lower temperatures, growth of the cubic material as a single phase was not observed. The existence of an apparent minimum in substrate temperature for the growth of pure c-BN indicates that the combination of thermal energy and intrinsic stress is insufficient for all the B and N atoms to surmount the activation energy barrier between the layered h-BN and the three-dimensional c-BN structure.

Similarly, an increase in ion flux and momentum transfer into the growing film will lead to a more rapid increase in stress, as shown by Kester and Messier [18] as well as Windischmann [25] and a decrease in the film thickness necessary for the initiation of the cubic phase. The results presented in Figs. 3(a) and (b) show the onset of c-BN to be also a function of ion flux. These correspondences between known effects on stress and the onset of c-BN growth are strong evidence that the cubic phase growth results directly from stress.

The mechanism(s) which cause(s) the increase in stress in the films is not completely understood. It may be densification due to ion bombardment, as reported by [27]. The

densification occurs through the collapse of the void structure found in non-bombarded films. Nir [28] and Targove and Macleod [29] have shown experimentally that the magnitude of the compressive stress is a function of the momentum transfer to the growing surface for particle energies <1kV. Theoretical studies by Windischmann [30] support these findings. A second possibility is that the stress is due to the presence of interstitials in the film. In the case of the c-BN films, the relatively high concentration of Ar (1.5 at.%) as shown by RBS would suggest that the compressive stress may be caused by interstitial Ar atoms in the manner observed by McKenzie *et al.* [14].

In the growth of BN films via IBAD by Stambouli et. al. [31] using bombardment with nitrogen ions, it was found that sufficient bombardment by nitrogen ions resulted in nitrogen-rich (non-cubic) BN_{1+x} films with a higher density than stoichiometric BN films. The former also possessed significantly higher compressive stresses than the stoichiometric films. They attributed this to interstitial N. If this is the case, bombardment by the larger Ar ion, and the formation of interstitial Ar at 1.5 at.%, would be expected to also increase the compressive stress in the films. In fact, Fahnline *et al.* [32] showed that 1.5 at.% Ar in Ge films caused a significant increase in compressive intrinsic stress.

Kester and Messier [18] previously showed that the phase of BN films is determined by three factors: substrate temperature, bombardment measured in terms of momentum transfer, and stoichiometry. The stoichiometry factor was a requirement in that at least one bombarding N atom had to be present for each depositing B atom. They plotted the observed phase(s) as a function of temperature and bombardment. In the present study we have shown that these are controlling parameters, but they control not only whether or not cubic growth will occur, but the time of nucleation and growth of this phase. Some of the conditions that they described as leading to mixed cubic and hexagonal growth appear to be conditions leading to layered single phase hexagonal followed by single phase cubic growth.

The problem of adhesion of c-BN on Si was addressed by using substrates with better lattice matching to c-BN including Cu and Ni and diamond. The cubic phase did not grow on the Cu(100) substrate due to its excellent ductility which adsorbed the stresses generated in the growing film; it did grow on the less ductile Ni(100) substrate, but the adhesion was as poor as on Si. These results indicate that the adhesion problem is not simply one of lattice mismatch with the substrate.

Adhesion on the diamond substrates was much better than on the other materials. Although a relatively small number of samples were produced, due to the prohibitive cost, these results suggest that c-BN does not easily grow initially on diamond even though this substrate has a higher surface energy than c-BN. Moreover, these results imply that c-BN will not initially deposit on any material, at least by the methods used in this investigation.

E. Conclusions

Boron nitride films deposited using ion beam assisted deposition on Si, diamond and Ni substrates grow in a sequence of amorphous, hexagonal and cubic layers. This is believed to be caused primarily by the increased incorporation of intrinsic biaxial compressive stresses in the films. The nucleation of the cubic phase occurs at differing film thicknesses as a function of both substrate temperature and ion flux. There appears to be a minimum substrate temperature (200–300°C) below which single phase growth of c-BN does not occur. At higher temperatures the onset of the cubic phase is a function of temperature, appearing at greater thicknesses at higher temperatures under the same ion flux. This is attributed to increased adatom mobility and bulk annealing with increasing temperature and a concomitant relaxation of stress. For these reasons the optimum temperature range for the growth of c-BN was determined to be 400-500°C. This range in T is similar to that determined by other investigators. Increased ion bombardment, as measured by momentum transferred into the film, leads to an earlier start of cubic growth, apparently due to the increased stress. It is suggested that the stress in the films may be due to Ar interstitials. The fact that stress is a function of momentum transferred into the film may be due to higher momentum bombardment (higher flux, energy or ion mass) leading to deeper and/or a greater number of interstitials.

We were unable to nucleate c-BN as the initial phase on any substrate; we suspect that this may prove difficult using bombardment based deposition methods due to the requirement of increasing stress generation in the films.

E. Acknowledgements

The authors express their appreciation to the Electronic Materials Center of Kobe Steel, USA and the Strategic Defense Initiative via the Office of Naval Research (Contract No. N00014-92-J-1720) for support of this research, to Dr. Nalin Parikh of the University of North Carolina-Chapel Hill for the RBS measurements, to Professor D. R. McKenzie of the University of Sydney and Lisa M. Porter, R. C. Glass and M. J. Paisley of NCSU for helpful discussion.

F. References

1. L. Vel, G. Demazeau, and J. Etourneau, Materials Science and Engineering **B10**, 149 (1991).
2. K. Era, O. Mishima, Y. Wada, J. Tanaka, and S. Yamaoka, in Electroluminescence, edited by S. Shionoya and H. Kobayashi, Springer Proceedings in Physics, **38**, 386 (1989).
3. R. H. Wentorf, Jr., J. Chem. Phys. **26**, 956 (1957).
4. V. N. Gashtold *et al.*, Elektronnaya Tekhnika **12**, 58 (1970).
5. K. Inagawa, K. Watanabe, H. Ohsone, K. Saitoh, and A. Itoh, J. Vac. Sci. Technol. **A5**, 2696 (1987).

6. D. J. Kester and R. Messier, Mater. Res. Soc. Symp. Proc. **235**, 721 (1992).
7. T. Wada and N. Yamashita, J. Vac. Soc. Technol. **A10**, 515 (1992).
8. K. Bewilogua, J. Buth, H. Hübsch, and M. Grischke, Diamond and Related Materials **2**, 1206 (1993).
9. M. Murakawa, S. Watanabe, and S. Miyake, Diamond Films and Technol. **1**, 55 (1991).
10. G. L. Doll, J. A. Sell, C. A. Taylor II, and R. Clarke, Phys. Rev. B **43**, 6816 (1991).
11. T. A. Friedmann, K. F. McCarty, and E. J. Klaus, Applied Physics Letters **61**, 2406 (1992).
12. Y. Osaka, M. Okamoto, and Y. Utsumi, Mater. Res. Soc. Symp. Proc. **223**, 81 (1991).
13. H. Saitoh and W. Yarborough, Applied Physics Letters **58**, 2228 (1991).
14. D. R. McKenzie, W. D. McFall, W. G. Sainty, C. A. Davis and R. E. Collins, Diamond Relat. Mater. **2**, 970 (1993)
15. D. R. McKenzie, J. Vac. Sci. Technol. **A11**, 2758 (1993).
16. M. Okamoto, H. Yokoyama, and Y. Osaka, Japanese Journal of Applied Physics **29**, 930 (1990).
17. D. J. Kester, K. S. Ailey, R. F. Davis, and K. L. More, J. Mater. Res. **8**, 1213 (1993).
18. D. J. Kester and R. Messier, J. Appl. Phys. **72**, 504 (1992).
19. W. Kern and D. A. Puo-tinen, RCA Rev. **31**, 187 (1970).
20. D. Van Vechten, G. K. Hubler, and E. P. Donovan, Vacuum **36**, 841 (1986).
21. R. Geick and C. H. Perry, Phys. Rev. **146**, 543 (1966).
22. P. J. Gielisse, S. S. Mitra, J. N. Plendl, R. D. Griffis, L. C. Mansur, R. Marshall, and E. A. Pascoe, Phys. Rev. **155**, 1039 (1967).
23. C. H. Carter, Jr., J. A. Edmond, J. W. Palmour, J. Ryu, H. J. Kim and R. F. Davis in *Microscopic Identification of Electronic Defects in Semiconductors,* edited by N. M. Johnson, S. G. Bishop, and G. Watkins (Mater. Res. Soc. Proc., 46, Pittsburgh, PA 1985) pp. 593 -598.
24. N. Tanabe, T. Hayashi, and M. Iwaki, Diamond and Related Materials **1**,151 (1992).
25. H. Windischmann, J. Vac. Sci. Technol. **A7**, 2247 (1989).
26. H. Windischmann, J. Appl. Phys. **62**, 1800 (1987).
27. R. A. Roy and D. S. Yee, in *Handbook of Ion Beam Processing Technology*, edited by J. J. Cuomo, S. M. Rossnagel, and H. R. Kaufman, (Noyes, Park Ridge, NJ, 1989).
28. D. Nir, J. Vac. Sci. Technol. **A4**, 2954 (1986).
29. J. D. Targove and H. A. Macleod, App. Optics **27**, 3779 (1991).
30. H. Windischmann, J. Vac. Sci. Technol. **A9**, 2431 (1991).
31. V. Stambouli, O. Burat, D. Bouchier, and G. Gautherin, Surface and Coatings Technology **43/44**, 137 (1990).
32. D. Fahnline, B. Yang, K. Vedam, R. Messier, and L. Pilione, Mater. Res. Soc. Symp. Proc. **130**, 355 (1989).

IV. Distribution List

Mr. Max Yoder Office of Naval Research Electronics Program–Code 314 Ballston Tower One 800 North Quincy Street Arlington, VA 22217-5660	3
Administrative Contracting Officer (Kathy L. Raible) Office of Naval Research Regional Office Atlanta 101 Marietta Tower Suite 2805 101 Marietta Street Atlanta, GA 30332-0490	1
Director Naval Research Laboratory Attention: Code 2627 Washington, DC 20314	1
Defense Technical Information Center Building 5 Cameron Station Alexandria, VA 22314	2